

UNCLASSIFIED

AD 415870

DEFENSE DOCUMENTATION CENTER

FOR

SCIENTIFIC AND TECHNICAL INFORMATION

CAMERON STATION, ALEXANDRIA, VIRGINIA



UNCLASSIFIED

NOTICE: When government or other drawings, specifications or other data are used for any purpose other than in connection with a definitely related government procurement operation, the U. S. Government thereby incurs no responsibility, nor any obligation whatsoever; and the fact that the Government may have formulated, furnished, or in any way supplied the said drawings, specifications, or other data is not to be regarded by implication or otherwise as in any manner licensing the holder or any other person or corporation, or conveying any rights or permission to manufacture, use or sell any patented invention that may in any way be related thereto.

C 3-4 + 00

(12) (13)
AFCRL-62-339 (II)

(7-5-4)

HARDENED POINT-TO-POINT
COMMUNICATION ANTENNA
CONFIGURATIONS.

(VOLUME II).

(10)

by W. T. Whistler, J. W. Stauffer, K. G. Schroeder,
R. C. Roden, L. H. Dee

ADVANCE PROJECTS DEVELOPMENT SECTION
HEAVY MILITARY ELECTRONICS DEPARTMENT
GENERAL ELECTRIC COMPANY
SYRACUSE, NEW YORK
PROJECT 4600
TASK 460007

(17)
MAY 1962

(14)
FINAL REPORT, NUMBER G.E.-R62EMH23
CONTRACT NUMBER: AF 19(604)-7469

PREPARED FOR
ELECTRONICS RESEARCH DIRECTORATE
AIR FORCE CAMBRIDGE RESEARCH LABORATORIES
OFFICE OF AEROSPACE RESEARCH
UNITED STATES AIR FORCE
BEDFORD, MASSACHUSETTS

(12) 30 P.
(13) 14
(20) 11
(21) 14

(15) 9

Requests for additional copies by Agencies of the Department of Defense, their contractors, and other Government agencies should be directed to the:

ARMED SERVICES TECHNICAL INFORMATION AGENCY
ARLINGTON HALL STATION
ARLINGTON 12, VIRGINIA

Department of Defense contractors must be established for ASTIA services or have their 'need-to-know' certified by the cognizant military agency of their project or contract. All other persons and organizations should apply to the:

U. S. DEPARTMENT OF COMMERCE
OFFICE OF TECHNICAL SERVICES
WASHINGTON 25, D. C.

TABLE OF CONTENTS

Section	Page
1.0 INTRODUCTORY NOTE	1
2.0 ABSTRACT	3
3.0 FACTUAL DATA	7
3.1 Fixed Coverage Hard Antennas	7
3.2 Ring Arrays	29
3.3 The Use of Scattering Matrices in the Measurement of Mutual Coupling	73

LIST OF ILLUSTRATIONS (Continued)

Figure		Page
27	Double Arc Arrays Producing Beams at Right Angle	47
28	Modular Ring Arrays Producing Three and Four Beams	49
29	48 Element Circular Array: Forming Two Overlapped Forward Beams	51
30	48 Element Circular Array: Pattern for Three Single-Arc Feeds	52
31	Experimental Model: Top View	58
32	Experimental Model: Bottom View	59
33	Volumetric Coverage of Ring Array	62
34	Change of Element Phase with Beam Direction	64
35	Individual Element Ground Plane Variations	69
36	Attenuation of Propagated Wave Due to Ground Losses	70
37	Ground Wave Propagation Improvement with Artificial Lake	71
38	$ S_{12} ^2$ vs. Distance of Separation between Dipoles	78
39	Transmission Efficiency	79
40	Reflection Losses in Antenna 1	80
41	Power Measured by Bolometer between Adjacent Dipoles	81

1.0 INTRODUCTORY NOTE

This study, AF 19(604)7469 (Hard Communications Antennas), is a companion study to a Melpar study AF 19(604)7357. After both contracts were awarded, the two programs were modified so that GE covered all antennas useful in the 100-1000 Mc band (hence, predominantly communication antennas) while Melpar covered all antennas in the 1000-10,000 Mc band (hence, mainly radar antennas). Information contained in the 7357 final report was available to General Electric, and there was a free interchange of ideas between the two contractors.

This final report is printed in one classified and one unclassified volume by customer request to permit wider dissemination of the unclassified antenna ideas presented.

2.0 ABSTRACT

A study has been conducted to determine the relative hardenability of various antenna designs in the 100-1000 Mc band. Circularly symmetric and point-to-point communication antennas were investigated.

The status of projects as outlined in six-month report (AFCRL 579) is as follows:

1. Two different flush-mounted Yagi designs were conceived and experimental models tested. These are the quarter-wave, post-image Yagi and the cavity-backed slot Yagi.
2. An IBM program for ring arrays was written and used to define the effects of element spacing on the patterns of full-ring and split-ring designs. An experimental model has been built.
3. Structural studies of quarter-wave posts and capped, folded monopoles were made to estimate overpressure limits of antenna designs employing them.
4. Several short environmental studies were made, including effects of lossy ground on pattern, thermal materials and heat transfer studies.

Studies completed and reported in final report period are:

1. Full scale pattern tests of 3 post-image Yagi antennas at 415, 1000 and 1800 Mc. Experimental evaluation of a 2λ backfire antenna.
2. A discussion of hardenability of communication antennas from the mechanical and thermal points of view.

3. ^{The} Design and hardenability of circularly symmetric arrays (e.g. elements in ring and star shaped configurations) ^{was investigated}

The use of scattering matrices in the measurement of mutual coupling is presented.

DETAILED TABLE OF CONTENTS FOR SECTION 3.1

	Page
3.1 Fixed Coverage Hard Antenna	7
3.1.1 Full-scale Pattern Measurements of Post Yagi Antennas	7
3.1.1.1 Description of Test Antennas	7
3.1.1.2 Description of Test Site	7
3.1.1.3 Description of Pattern Techniques and Measuring Equipment	9
3.1.1.4 Experimental Results	12
3.1.1.4.1 Measurement Coordinates	12
3.1.1.4.2 Index of Results	12
3.1.1.4.3 Discussion of Results	25

3.0 FACTUAL DATA

3.1 Fixed Coverage Hard Antennas

3.1.1 Full-scale Pattern Measurements of Post Yagi Antennas

The design, as regards hardness, and the measured performance of several hardened scale model Yagi antennas were presented in the first Semi-Annual Report on this contract.⁽¹⁾

Since the radiation characteristics of a flush mounted endfire antenna are strongly influenced by the physical environment of the site, it was deemed necessary to measure the performance of an operational "hardened" antenna. This was done and the results of the measurements are presented in this section.

3.1.1.1 Description of the Test Antennas

The antennas under test were post-type half-Yagis. Three antennas were constructed, each to operate at a frequency of 1800, 1000, and 415 mcs respectively. The electrical design was such as to accommodate mechanical hardness. The height-to-diameter ratio of the director elements was 1.2. The length of the radiating structure was 4λ , and the measured free-space gain was 16db above isotropic.

The reflector, feeder, and director elements were mounted upon a 1/32" thick aluminum sheet which was secured to an 8' x 16' tiltable ground plane. This arrangement permits the plane of the radiating structure to be tilted an angle δ with respect to the earth's surface.

3.1.1.2 Description of the Test Site

A general view of the test site at Electronics Park, Syracuse, looking in the direction of propagation, is shown in Figure 1. The choice of the test site was dictated primarily by availability. As can be seen from the photo, the site is not free of obstructions in the direction of propagation. Several large trees are located about 400 feet in front of the antenna. These trees are about 50 feet high, and their foliage at the time the measurements were made was not dense enough to obstruct vision. Beyond the trees, at a distance of 520 feet from the antenna, is an 8-foot high woven wire fence. The elevation angle of the top of the fence as observed from the location of the antenna is about 0°. Beyond the fence (about 1000 feet in front of antenna) directly in the propagation path lies a large Quonset type structure. The outer covering of the structure is galvanized sheet metal. This building is surrounded by a dense grove of pine trees. The site is free from obstructions on both sides and to the rear of the radiating structure. Suffice it to say that this environment presents an intriguing and challenging propagation problem.

(1) "Hardened Point-to-Point Communication Antenna Configurations", W. T. Whistler, et al; first Semi-Annual Scientific Report Contract Number: AF 19(604)-74-69; pp. 18-35.



Figure 1. General View of Test Site

To avoid the influences of the foreground obstructions upon the pattern measurements, a directive receiving antenna was used to sample the radiated pattern of the test antenna. The measurements were made at a range of 250 feet, which placed the receiving horn between the test antenna and the obstructions.

Figure 2 is a photograph of the ground plane installation. The radiating structure is mounted upon the 8' x 16' tiltable ground plane. The forward end of the tiltable plane can be elevated either 4" or 8" above the level of the ground. The wire mesh ground plane is secured to the earth with wooden pegs. The mesh is bonded to the tiltable ground plane to insure good electrical continuity.

The center section of the wire mesh ground plane is 23 gauge 1/4" mesh hardware cloth. This material covers an area of 25' wide and 50' long. The outer portion of the mesh ground plane is 1" mesh poultry netting (diamond shaped mesh). The over-all size of the mesh ground plane is 50' wide and 100' long. The electrical size of the ground screen for the different operating frequencies is summarized below:

Frequency (mcs)	Electrical Size of 1/4" mesh gnd. screen	Over-all Electrical size of gnd. screen
1800	46 λ wide x 92 λ long	91 λ wide x 180 λ long
1000	25 λ wide x 50 λ long	50 λ wide x 100 λ long
415	17 λ wide x 34 λ long	21 λ wide x 42 λ long

3.1.1.3 Description of the Patterning Techniques and Measuring Equipment

The radiation patterns of the antennas under test were determined by positioning a receiving antenna at discrete, known positions in the radiated field. Thus a display of the received power level, as a function of the position of the receiving antenna, is the relative power pattern of the test antenna.

The receiving system was lifted by a balloon and stabilized in the desired predetermined position by means of guy lines controlled on the ground. Under favorable weather conditions; i. e., wind speeds less than 5 m.p.h., this technique proved to be an effective method of positioning the receiving system. As an indication of the stability of the receiving antenna, the measurements of relative power levels at any given location were repeatable within $\pm \frac{1}{4}$ db.

For all the pattern measurements, the transmitting antenna (the antenna under test) was excited as indicated in Figure 3. For all measurements, the antenna was matched for the condition of minimum reflected power. The directivity of the coupler was about -30 db, which establishes the best match attainable. The transmitted and reflected power levels were monitored during all the pattern measurements to insure that the radiated power level remained constant.



Figure 2. Ground Plane Installation

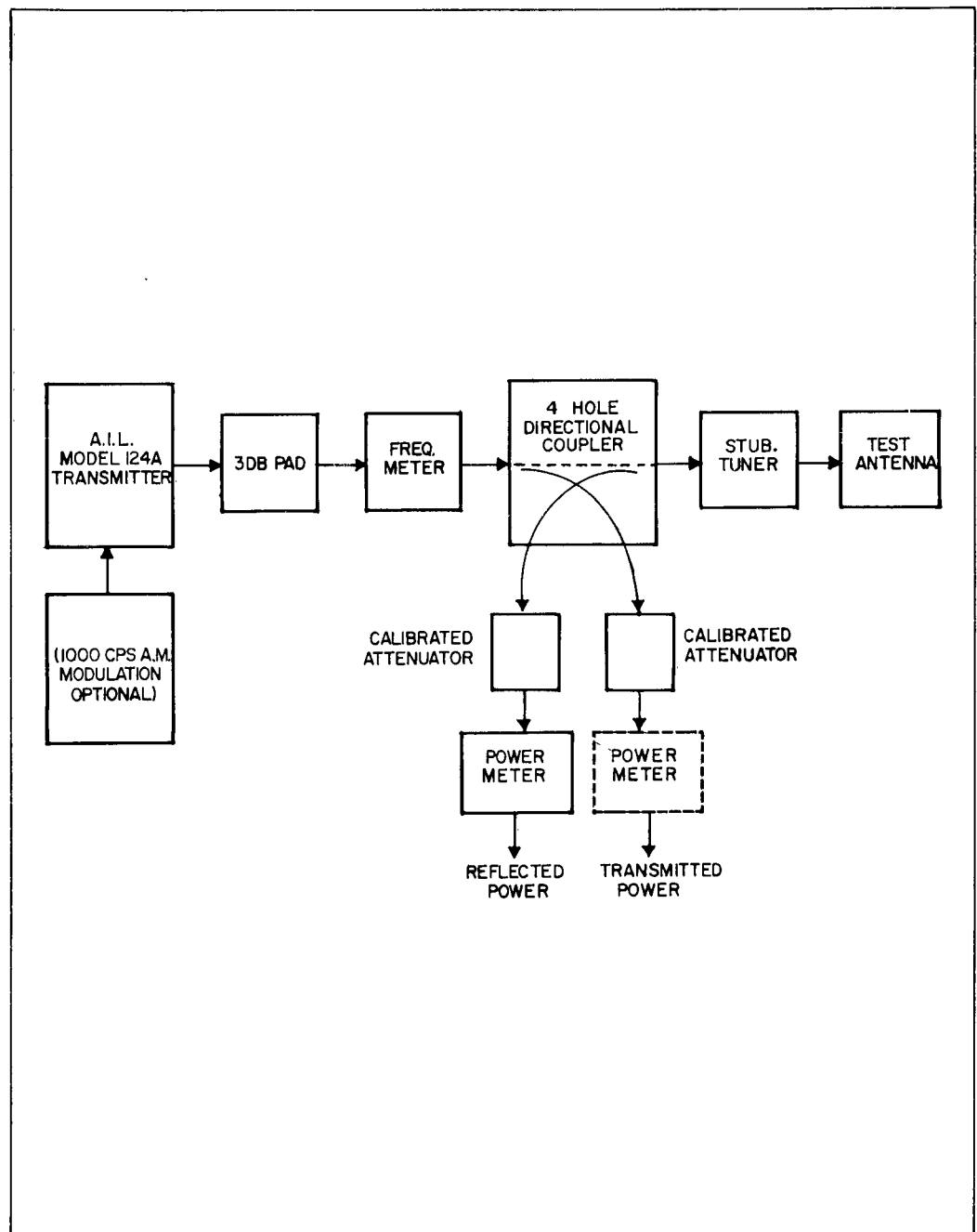


Figure 3. Functional Block Diagram of Transmitting Equipment

Since the lift capacity of the balloon was limited, it was convenient to use different receiving systems at the different frequencies. These systems are defined in Figures 4 and 5. It was necessary to use a directive receiving antenna at the 1800 mc and 1000 mc frequencies in order to avoid the influences of reflections. (These reflections were not noticeable at the 415 mc frequency.) The half-power beamwidth in the elevation plane of the receiving horn was about 45°. Thus it was sufficient to maintain the receiving horn level in the elevation plane as it was raised in altitude. The relative azimuth position of the receiving horn was controlled from the ground and always pointed toward the transmitting antenna. Observe that the system shown in Figure 4 does not permit measurement of the absolute level of received power.

The receiving system used at 415 mcs is shown in Figure 5. This arrangement permits measurement of the absolute level of the received signal. For the gain measurements, the NF-105 was calibrated as a two-terminal R. F. voltmeter.

3.1.1.4 Experimental Results

3.1.1.4.1 Measurement Coordinates

The measurement coordinates are shown in Figure 6. Markers were located on the ground at a constant distance of 250 feet from the antenna. These were spaced at 4 degree increments in azimuth. For all elevation angles, the receiving antenna was stabilized in a position directly above a given azimuth marker. The change in range as a function of elevation angle amounted to only 0.7 db in terms of relative power level at the maximum elevation angle of interest. This small change was considered negligible, and the relative power levels were not adjusted to account for the small range difference.

3.1.1.4.2 Index of Results

The graphs and tables which follow contain the following:

- i. Figures 7 thru 10 are the measured patterns of the 1800 mc antenna.
- ii. Figures 11 and 12 are the patterns of the 1000 mc antenna.
- iii. Figure 13 shows the measured patterns of the 415 mc antenna.
- iv. The table on page 24A contains a summary of pattern parameters.
- v. Figure 14 compares the expected and measured results regarding beam tilt as a function of ground plane size.
- vi. Figure 15 shows the patterns of the 415 mc antenna with various amounts of dirt deposited upon the radiating structure.

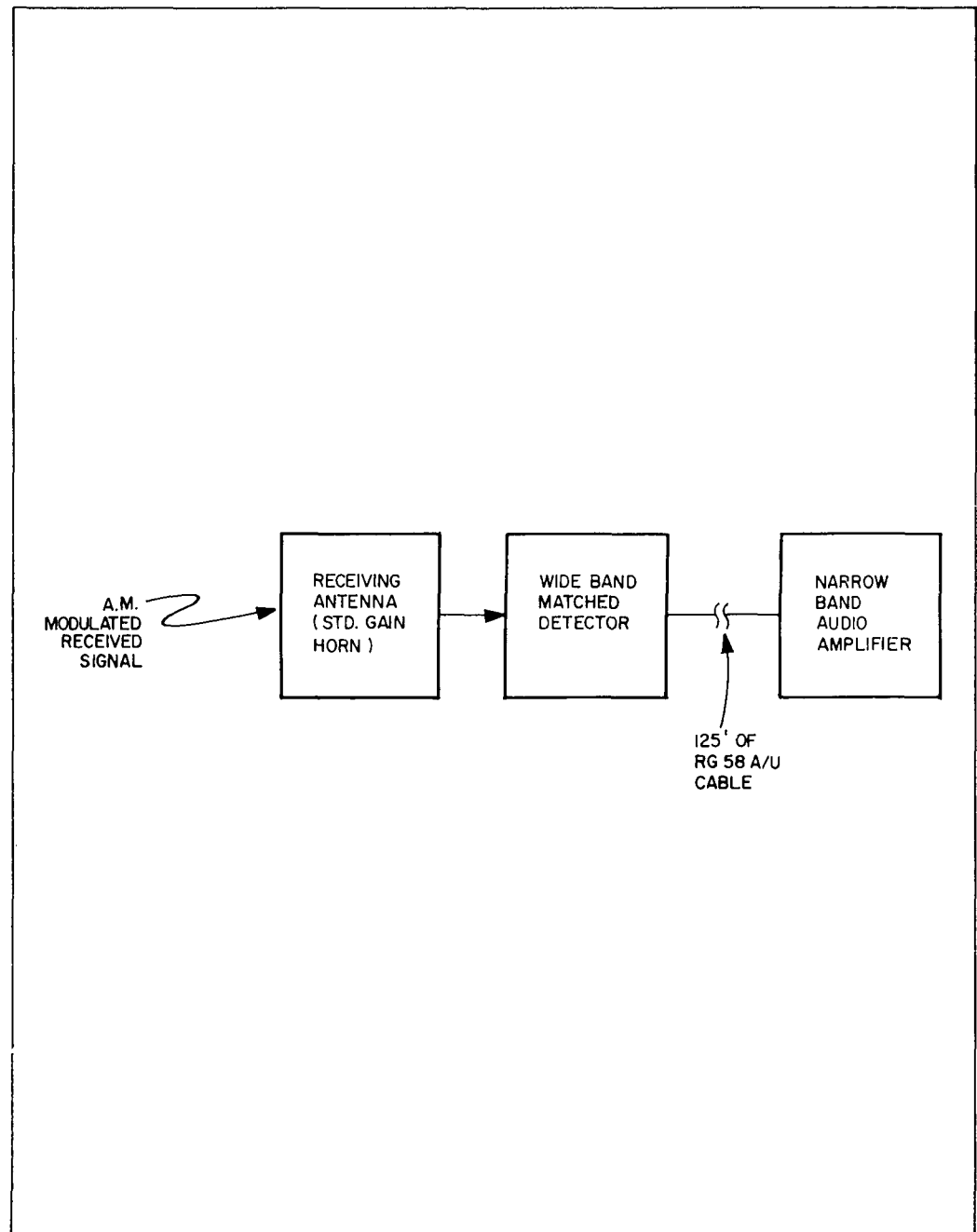


Figure 4. Receiving System Used For The 1800 Mc and 1000 Mc Pattern Measurements

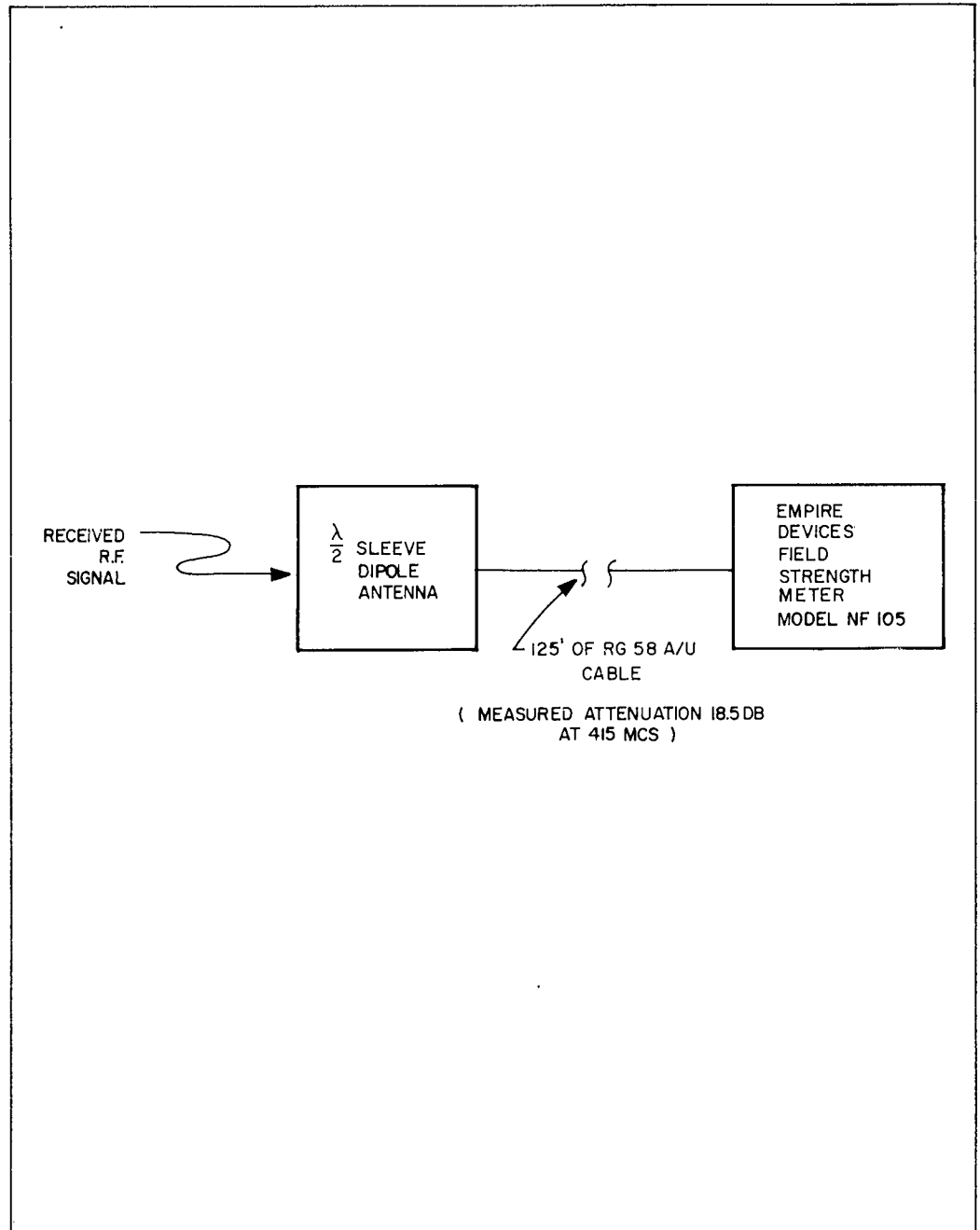


Figure 5. Receiving System Used For The 415 Mc Pattern Measurements

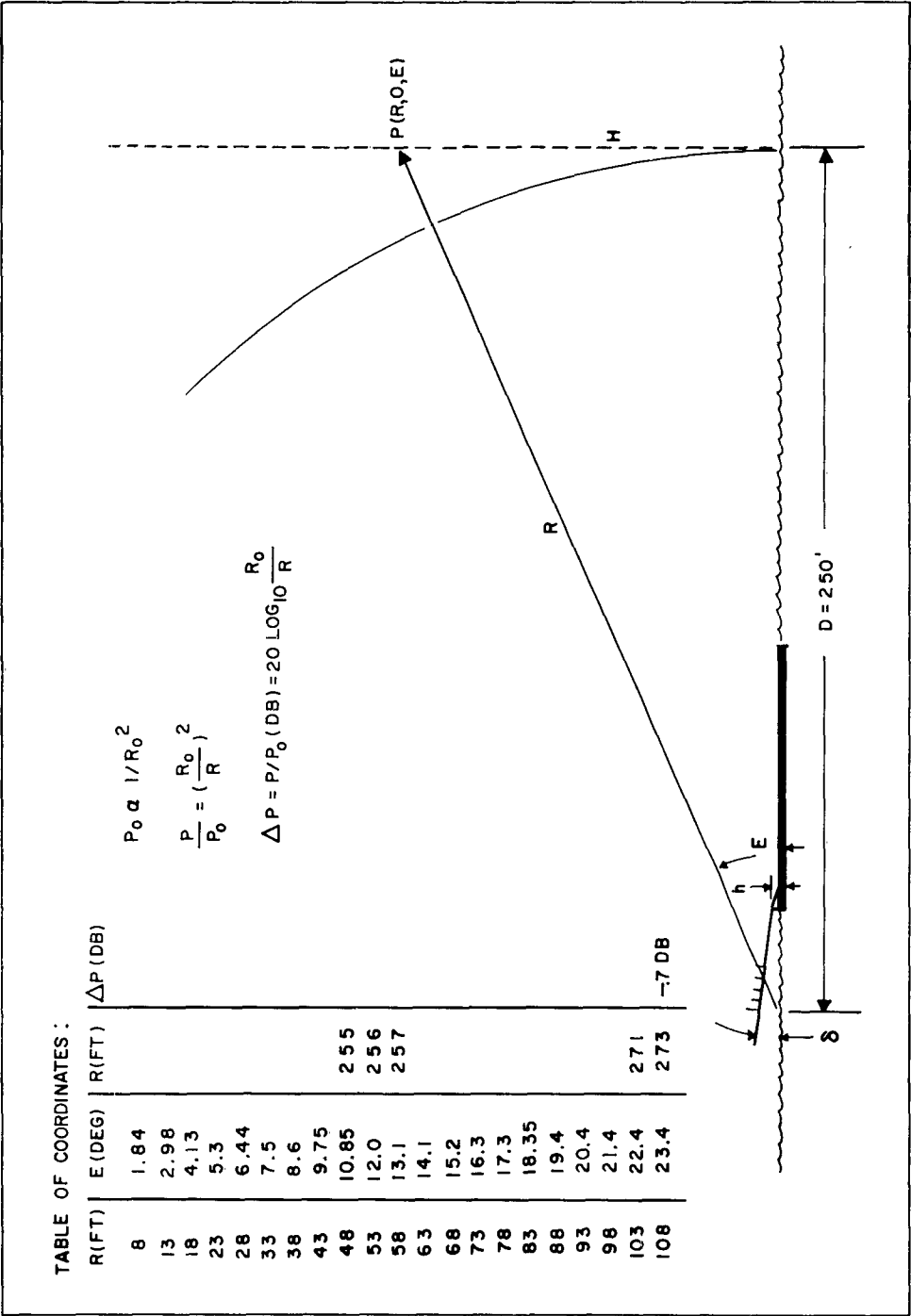


Figure 6. Measurements Coordinates

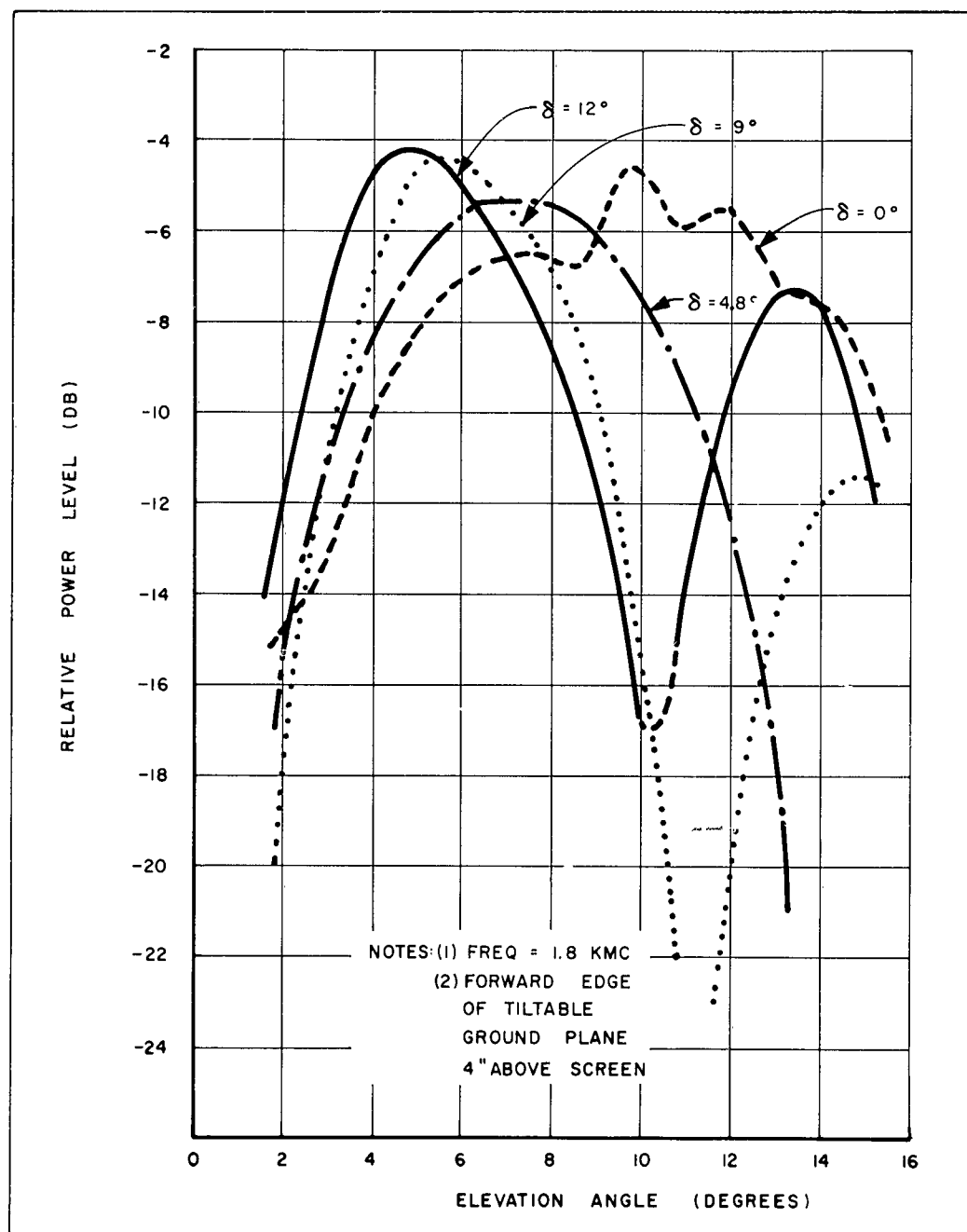


Figure 7. Principal E-Plane Patterns for Various Ground Plane Tilts

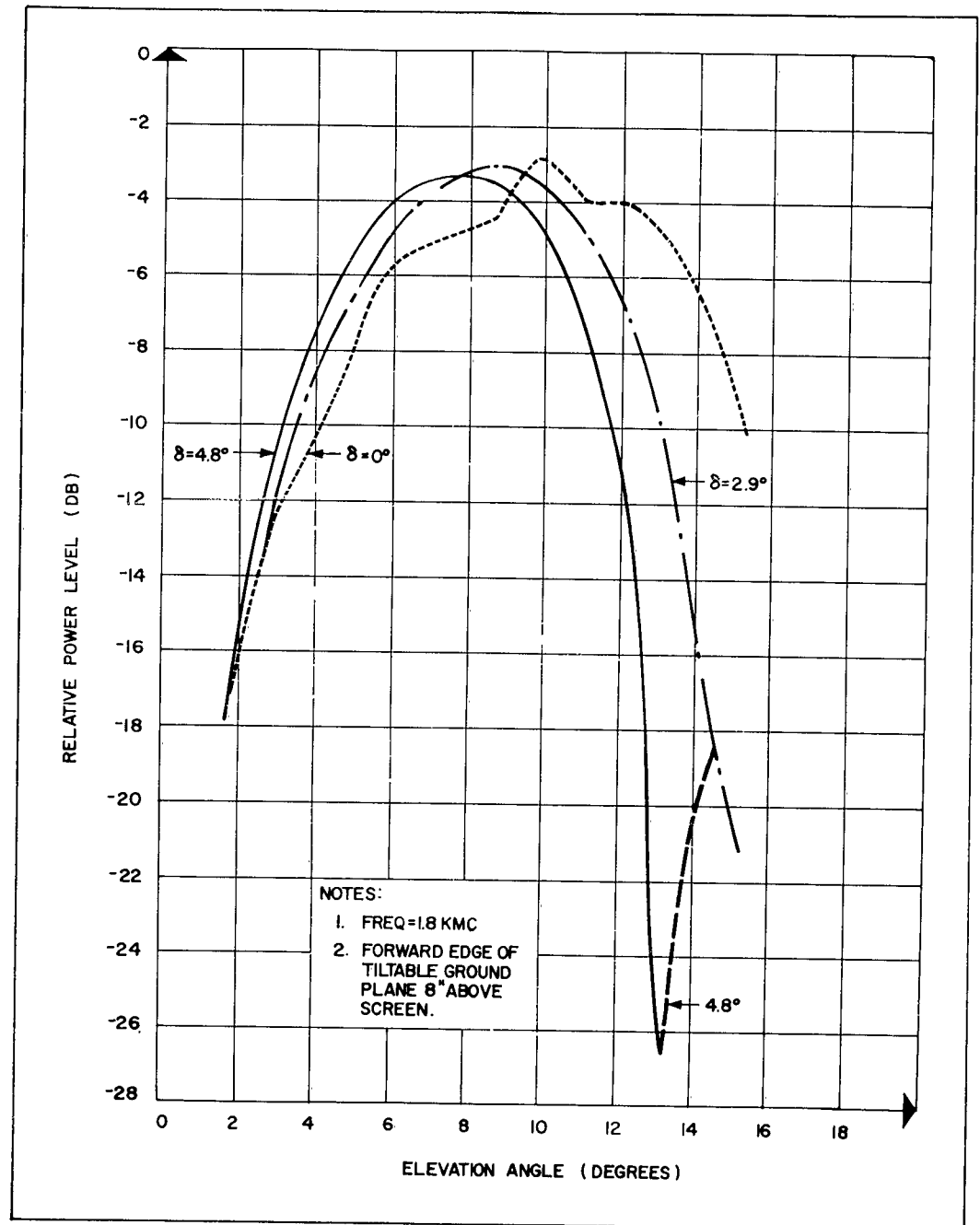


Figure 8. Principal E-Plane Patterns for Various Ground Plane Tilts

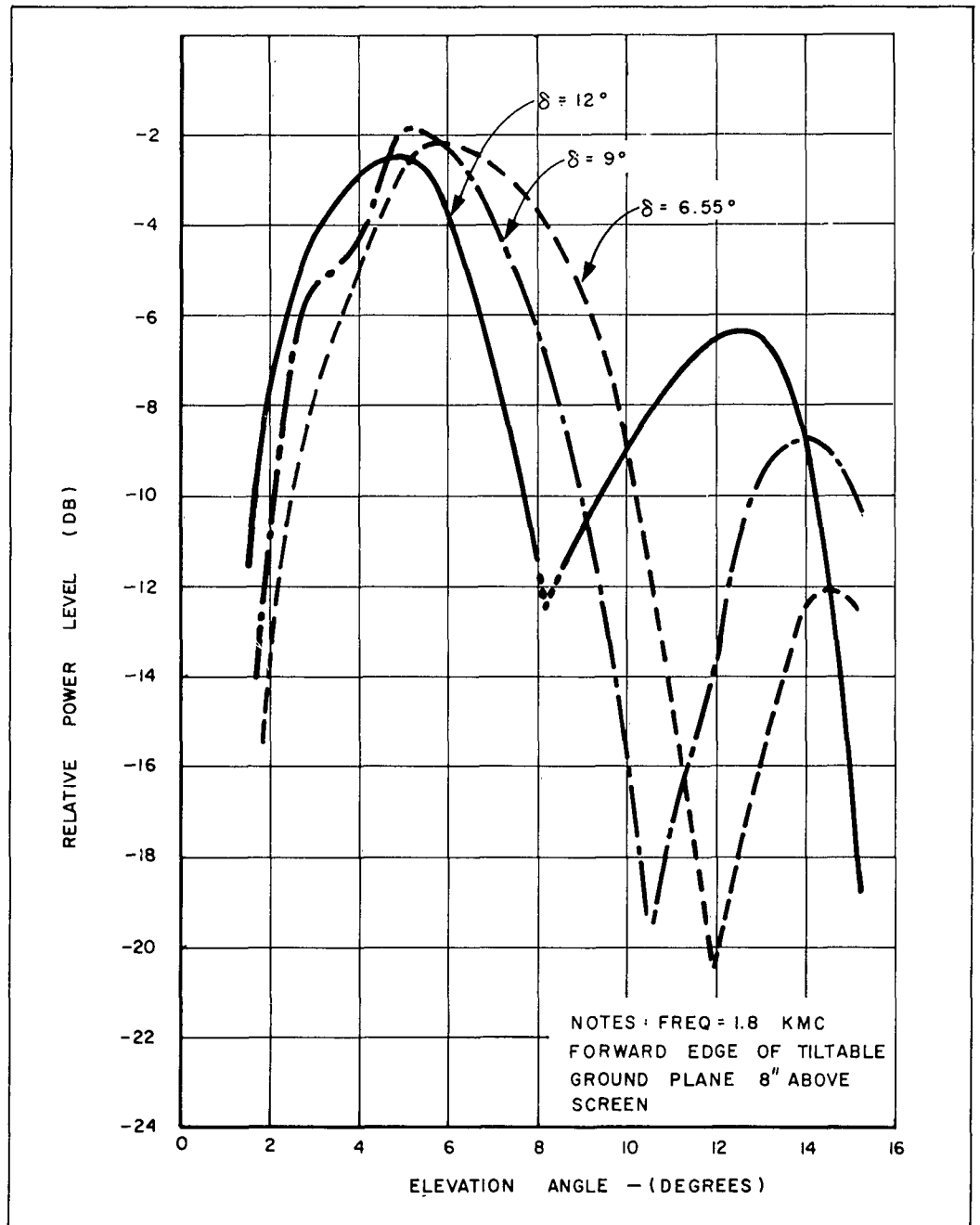
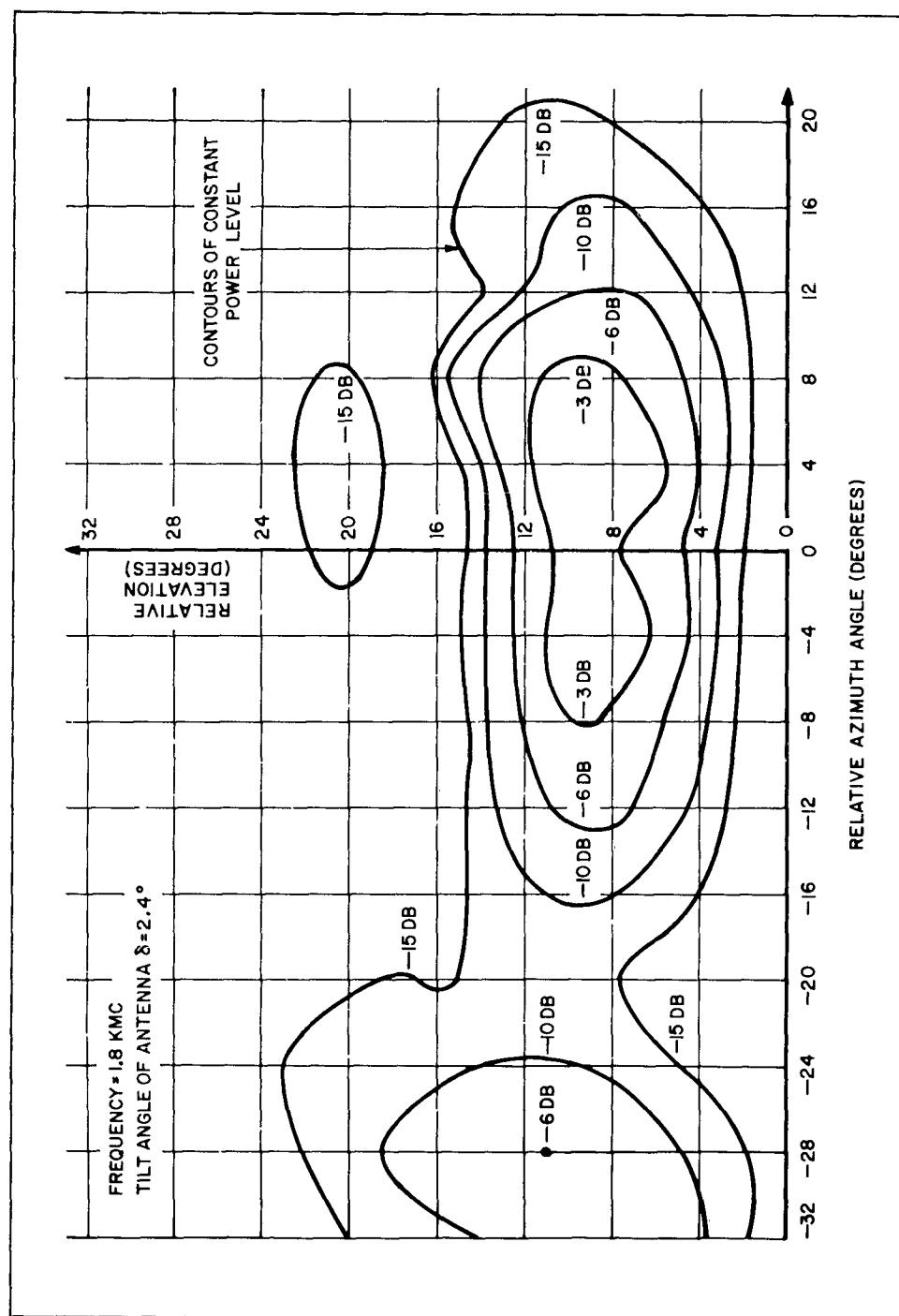


Figure 9. Principal E-Plane Patterns for Various Ground Plane Tilts.



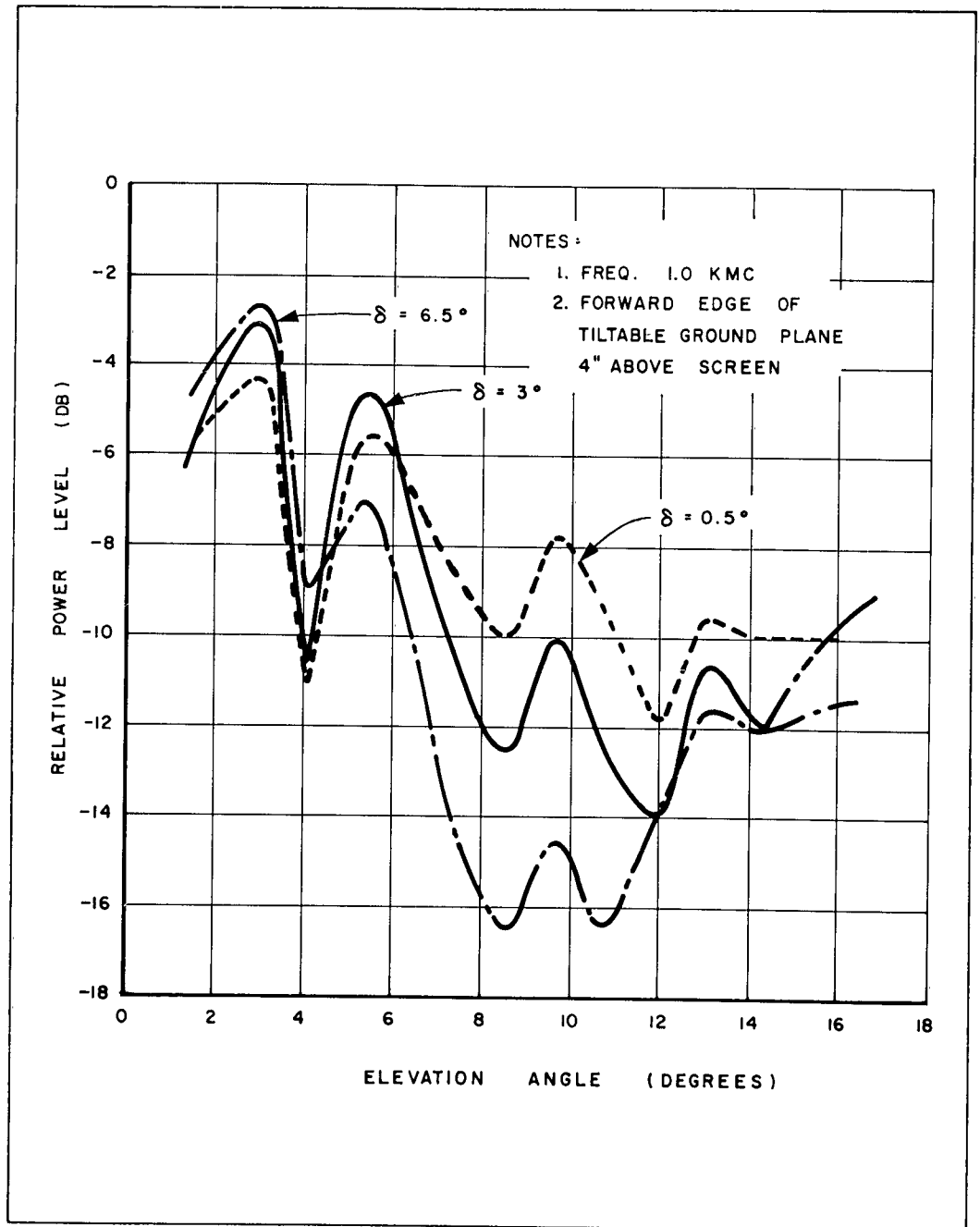


Figure 11. Principal E-Plane Patterns for Various Ground Plane Tilt Angles

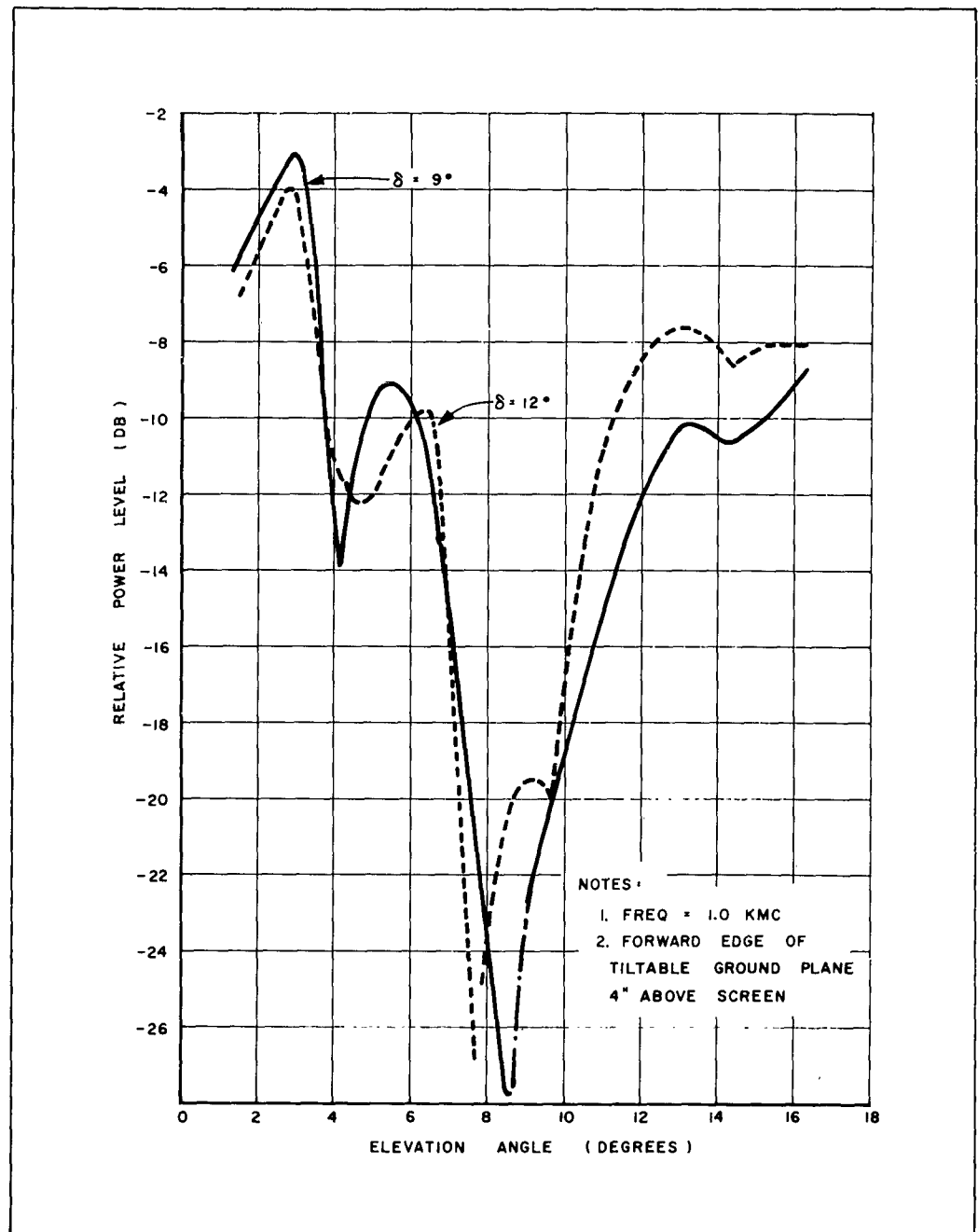


Figure 12. Principal E-Plane Patterns for Various Ground Plane Tilt Angles

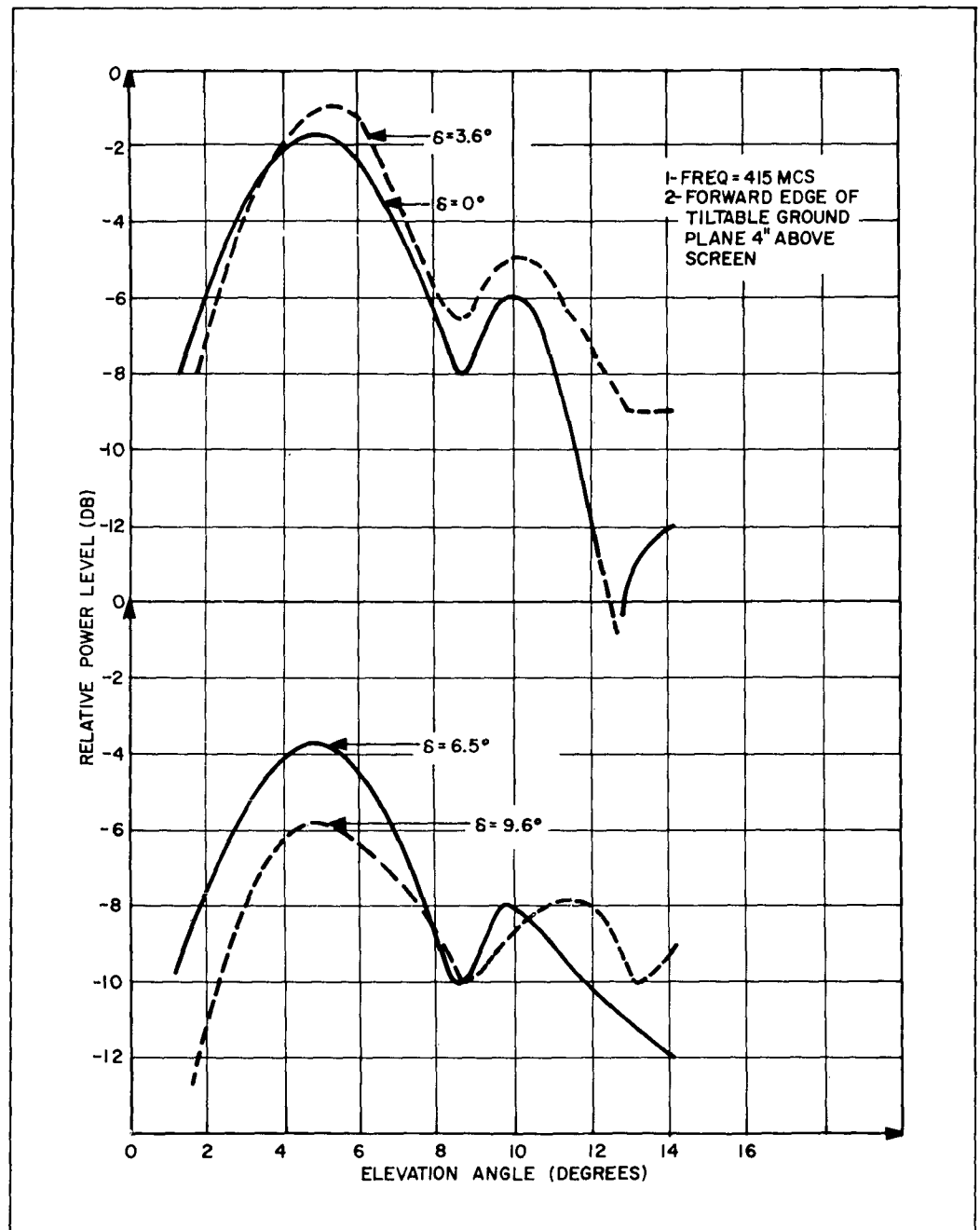


Figure 13. Principal E-Plane Patterns of 4λ Yagi Antenna for Various Ground Plane Tilt Angles (δ)

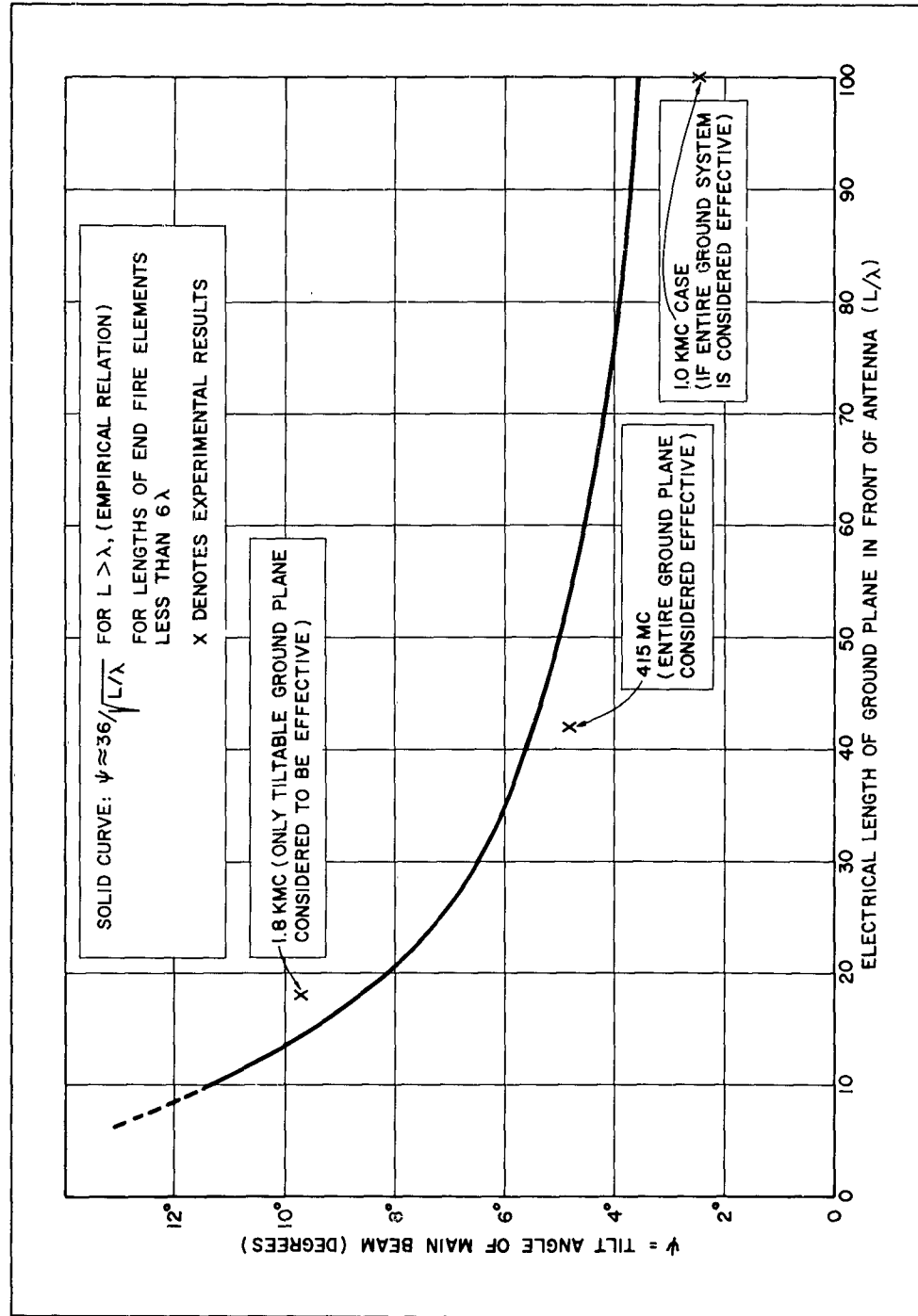


Figure 14. Effect of Ground Plane Length Upon the Elevation Position of the Main Beam

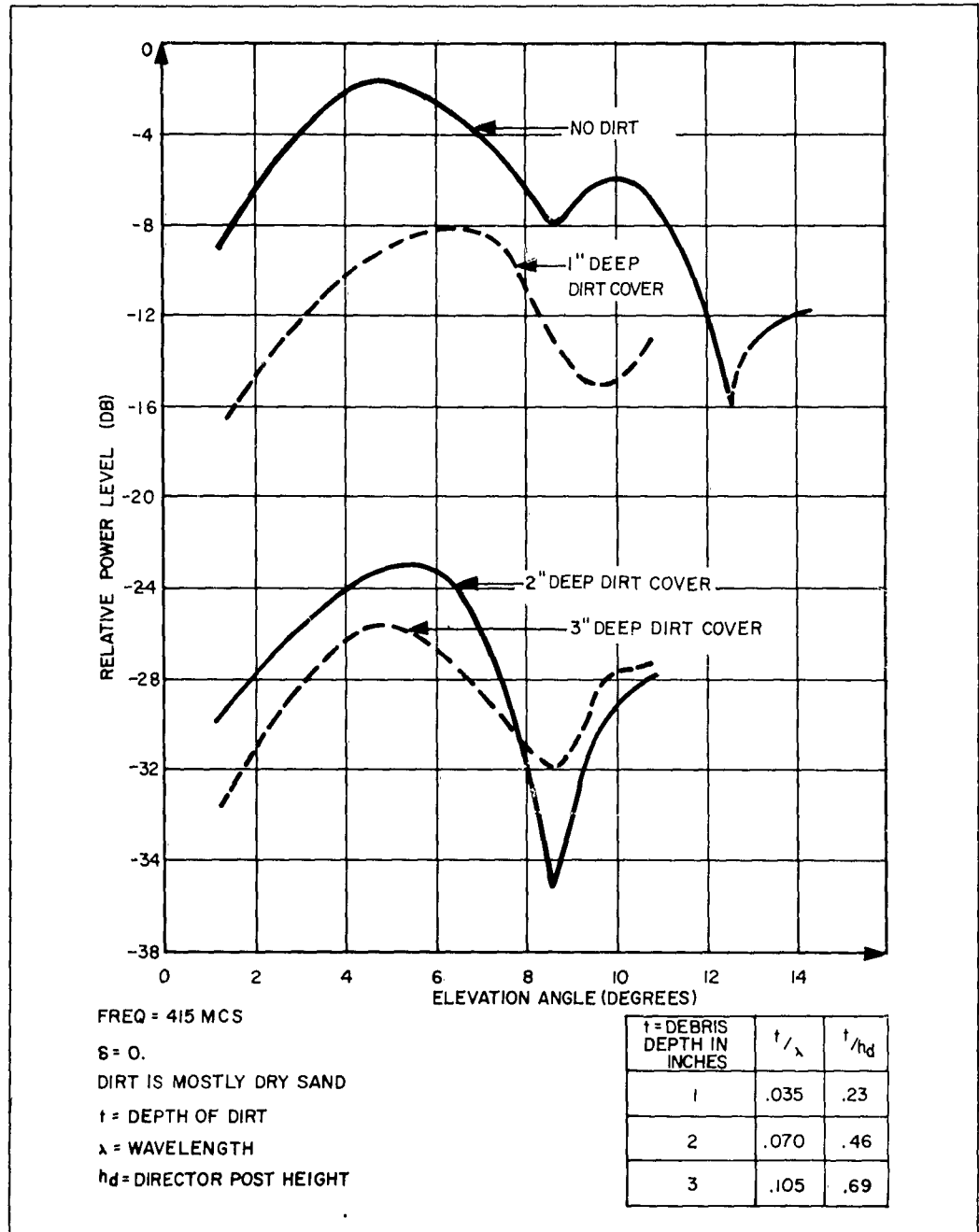


Figure 15. Principal E-Plane Patterns with Varying Amounts of Dirt Upon the Radiating Structure

SUMMARY OF PATTERN PARAMETERS

Freq. mcs	Ground Plane Angle δ (Deg.)	h = 8 inches			h = 4 inches		
		Half-Power Beamwidth in Elevation (Degrees)	Elevation Position of Beam Maximum ψ (Degrees)	Angular Position 1st Null in Elevation Pattern (Degrees)	H. P. B. W. Deg.	Elevation Position of Beam Maximum (Degrees)	Angular Position of 1st Null in Elevation Pattern (Degrees)
1800 ↓	0	8.0	9.8	----	8.0	9.5	----
	2.9	6.6	8.3	15.5	---	---	----
	4.8	6.1	7.5	13.2	6.4	7.2	13.5
	6.5	5.0	6.5	12.0	---	---	----
	9.0	4.0	5.6	10.5	4.4	6.2	11.5
	12.0	3.9	4.7	8.4	4.4	5.3	10.2
1000 ↓	0.5	Same as h = 4"			2.5	2.4	4.2
	3.0				2.1	2.5	4.2
	6.5				2.7	2.3	4.2
	9.0				2.1	2.6	4.2
	12.0				1.9	2.5	4.8
415 ↓	0	Same as h = 4"			4.7	4.8	8.6
	3.6				4.1	5.1	8.6
	6.5				4.7	4.8	8.6
	9.6				5.2	5.4	8.6

3.1.1.4.3 Discussion of the Results

The patterns of the 1800 mc and 1000 mc antennas were measured on the pattern range, before field installation, in order to verify the design. The "free space" gain was about 16 db above isotropic and the principal plane half-power beamwidths were 20° in azimuth and 14° in elevation. These values are about optimum for the 4λ length antenna. The patterns of the 415 mc antenna were not measured on the range because of the awkward size. The design parameters for this antenna were scaled according to frequency from the 1800 mc design data.

From the measured 1800 mc patterns (see Table at end of Section 3.1.1.2), the following observations should be made:

1. The half-power beamwidth of the elevation pattern decreases as the angle δ is increased.
2. As δ is increased, the entire elevation pattern shifts downward toward the horizon. (This is evident by the fact that the angular position of the nose of the beam, the first null and the peak of the first side lobe of the elevation pattern move downward together.)
3. Changing the height of the front edge of the tiltable ground plane from 4" to 8" had a negligible effect upon the pattern.

These observations lead one to the conclusion that at a frequency of 1800 mcs the mesh ground plane is not effective. A possible explanation of this behavior is that the ground screen was not sufficiently smooth, but instead was rough enough to behave as a diffuse reflector. Indeed there were ripples in the ground screen. The peak to peak amplitude of some of these ripples were on the order of $\lambda/2$ at a frequency of 1800 mcs.

There is, however, some evidence of reflection from the ground screen. Observe that as δ is increased the nulls in the elevation patterns are filled in and the amplitude of the first side lobe increases. A small amount of reflected energy will produce a marked effect in the side lobe structure. However, an appreciable narrowing of the main beam, as was observed, can be explained only on the basis of interference between a direct and reflected wave of about equal magnitude.

The 1000 mcs patterns are not easily explained. Note that the elevation position of the major lobe, which will be identified as the main beam, does not change as the angle δ increases. The half-power beamwidth is quite narrow, about 2.5° and remains nearly constant as a function of δ . Changing the height of the forward end of the tiltable ground plane from 4" to 8" above the level of the ground screen had no appreciable effect upon the pattern.

The pattern was checked at a range of 100 feet, which placed the receiving horn over the ground screen. The pattern measured at this location was essentially the same as those shown in Figures 11 and 12.

It should be recalled that the 1000 mc antenna was measured on the antenna range and its "free space" performance was identical to that of the 1800 mc antenna. Therefore, the odd performance observed in the field must necessarily be caused by the siting arrangement. No adequate explanation for the observed behavior has been found.

The 415 mc antenna patterns are as expected. Note from Figure 13 that the elevation position of the nose of the main beam does not change with increasing δ . However, observe that the peak relative power level of the main beam decreases as δ increases, indicating a loss in antenna gain with increasing δ .

DETAILED TABLE OF CONTENTS FOR SECTION 3.2

	Page
3.2 Ring Arrays	29
3.2.1 Multiple Ring and Star Arrays	29
3.2.1.1 General Considerations	29
3.2.1.2 Systematic Element Thinning in Multi-ring Arrays	31
3.2.1.3 Star Arrays	33
3.2.1.4 Conclusions	40
3.2.2 Multi-beam Operation of Modular Circular Array	40
3.2.2.1 Beams at Right Angles	46
3.2.2.2 Beams at Arbitrary Angles	48
3.2.2.3 Summary of Multiple Beam Modular Array	50
3.2.2.4 Experimental Results	57
3.2.3 Pattern of a Multi-ring Array of Isotropic Sources from Superposition of the Contributions of the Individual Elements	57
3.2.3.1 Plane Ring Arrays	57
3.2.3.2 Generalized Array with Arbitrary Ring Envelope	60
3.2.4 Operational Problems of Circular Arrays with Maximum Radiation Near Horizon	63
3.2.4.1 Electric Scanning over Limited Angular Range	63
3.2.4.2 Effect of Phase Errors	65
3.2.4.2.1 Systematic Errors	65
3.2.4.2.2 Random Phase Errors	65
3.2.4.3 Effects of Ground Conditions on Element Pattern	65
3.2.4.4 Pattern Deterioration in the Far Field	68

3.2 Ring Arrays

3.2.1 MULTIPLE RING AND STAR ARRAYS

3.2.1.1 General Considerations

Large diameter circular arrays are especially suited for satellite and space communications, where high-gain antennas are required. By using a combination of elements, e.g., an endfire dielectric antenna and a caploaded folded monopole, essentially hemispherical coverage can be achieved, one set of elements being scanned to ± 30 degrees from zenith, the other from there on down to horizon. If both elements were at the same location, a minimum-mutual-coupling element arrangement could be found, for instance, by feeding the dielectric endfire elements through the folded portion of the folded monopole. (Figure 16)

The two elements would not have to operate at the same frequency.

For optimum sidelobe conditions, it also may be required to use a different array configuration for the two extreme cases of beam position: operation at zenith and operation at horizon.

Since a single ring of the diameter required for the desired beamwidth would have -8 db sidelobes around zenith, and can only be improved to ~ -15 db at horizon*, it is more or less imperative to use a continuous circular aperture for good sidelobe suppression. For a circular grid of elements spaced half a wavelength, the number of elements becomes very large for any reasonably large diameter. For instance, if we have an array of 20 wavelengths diameter, which would result in a beamwidth at zenith of about 2 degrees, then we need 20 rings, spaced half a wavelength apart, with a total number of 1281 elements. This number is obtained by assuming 20 rings with a diameter

$$D_m = m \cdot \lambda$$

and a number of elements per ring:

$$N_m = 6m + 1$$

with

$$m = 0, 1, 2, 3, \dots, M$$

The total number of elements is then

$$\sum_{m=0}^M N_m = N_M = \frac{M+1}{2} (2+6M)$$

*See SEMI-ANNUAL REPORT, pp. 44-46.

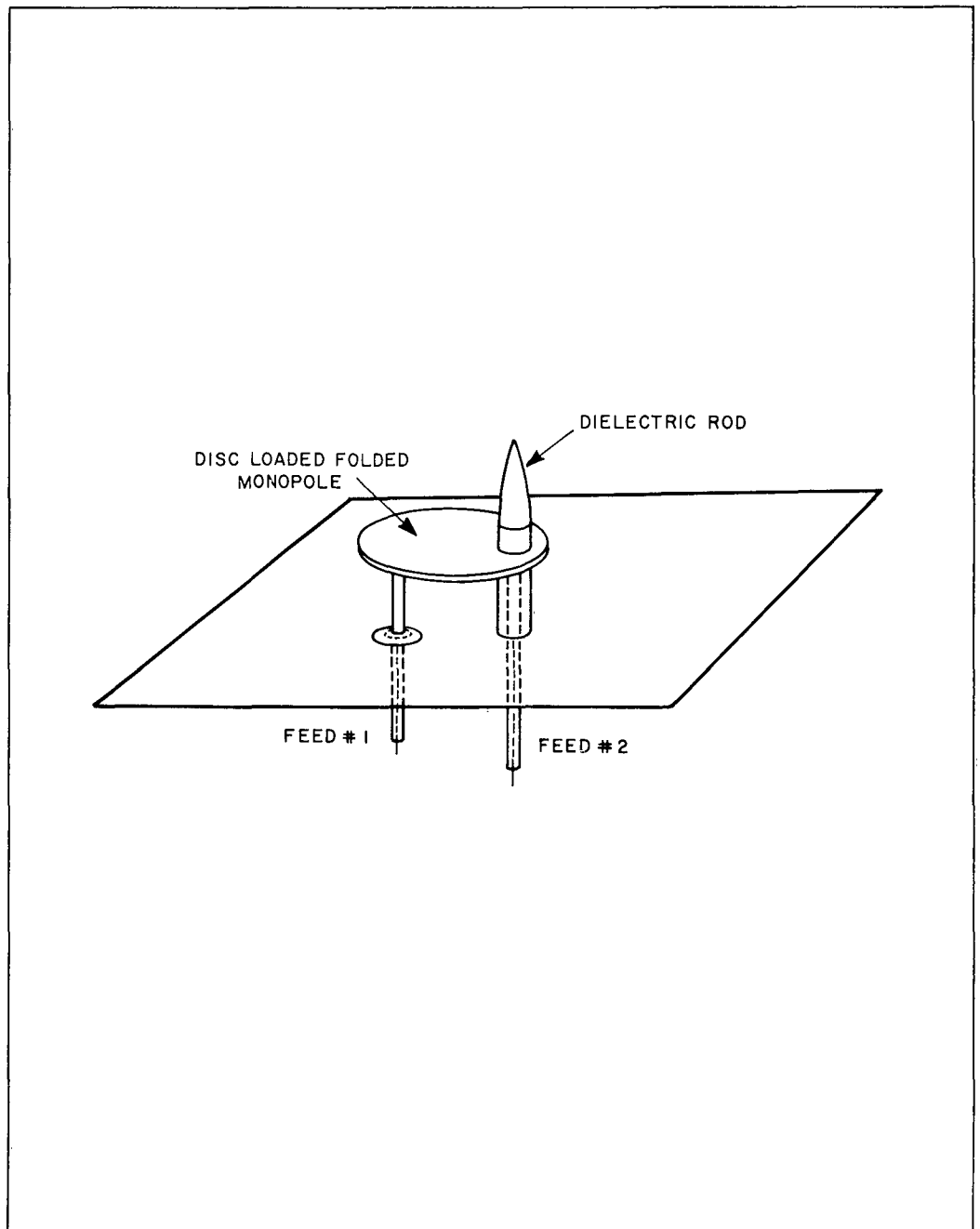


Figure 16. Combination Element for Ring Arrays

The formula for N_m is obtained by dividing the circumference of the consecutive rings by the element spacing on the rings, or half a wavelength, and then taking the next higher integer in order to assure that the element spacing on each ring is a little smaller than half a wavelength.

(Actually, the diagonal spacings within the circular grid are larger than half a wavelength, but this is of minor importance because, as far as interference is concerned, the diagonal spacing is cut in half by the other two adjacent elements of the grid.)

Now, it appears desirable to investigate the possibility of leaving out elements either in a random fashion, or by systematically increasing either the element spacing on the rings or the spacing from ring to ring.

Preliminary investigations showed that there is no advantage in nonuniform ring spacing and that amplitude weights applied to the aperture from ring to ring (each ring having the same amplitude for all elements) only improve the sidelobes in the broadside case, i.e., when the beam is pointing at zenith. In this case, for a "grid spacing" of up to 0.75λ no deterioration of the elevation pattern will occur, and the near-angle sidelobes can be improved over the -17.5 db for a continuous circular aperture by applying the necessary amplitude weights. The behavior of various arrangements of rings and elements on the rings has been investigated theoretically by using the computer program discussed in Sections 3.2.3 and 3.2.4.

The various problems arising for systematic element thinning are discussed in the following section.

3.2.1.2 Systematic Element Thinning in Multi-Ring Arrays

In any array of many rings, spaced a certain constant distance apart, sidelobe enhancement (echelon lobes) will occur in azimuth for a certain angle off the main beam direction at which the path difference from the elements on the ring diameters perpendicular to the beam direction becomes equal to one wavelength. This path difference is given by (See Figure 17)

$$d_\lambda = \Delta R_\lambda \sin \phi \sin \theta$$

where

d_λ = path difference in wavelengths

ΔR_λ = ring spacing in wavelengths

ϕ = azimuth angle off the beam axis

θ = elevation angle of the beam axis off zenith

The critical angle at which the secondary lobes occur (for a critical path difference $d_{\text{crit}} = 1\lambda$) is then given by

$$\phi_{\text{crit}} = \sin^{-1} \left(\frac{1}{\Delta R_\lambda \sin \theta} \right)$$

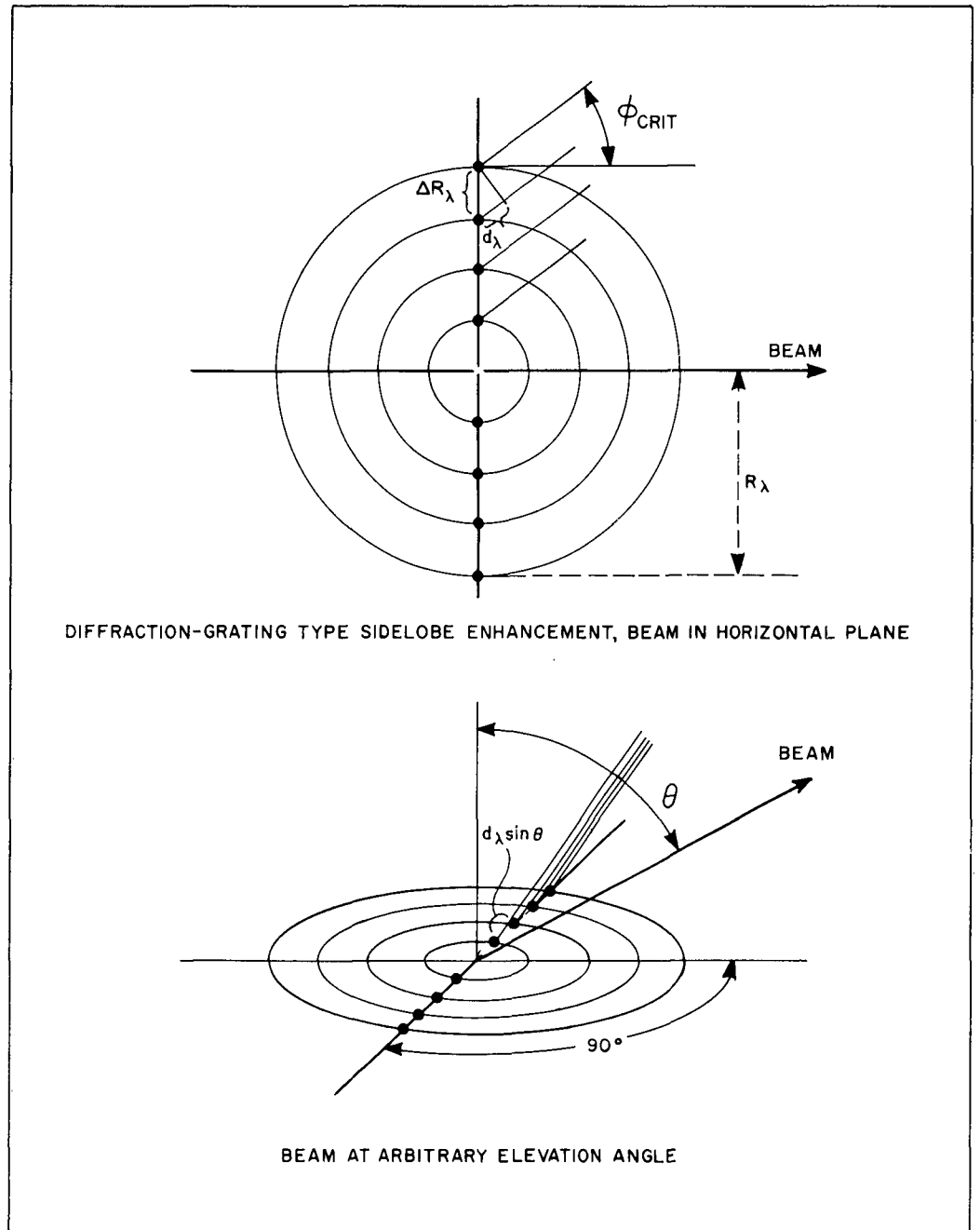


Figure 17. Ring Problem Geometry

As an example, the sidelobe patterns for a 20λ maximum diameter, 5-ring circular array with the beam pointing at horizon all show secondary lobes at ± 30 degrees, which agrees with the critical angle from the above formula for $\theta = 90^\circ$. ($\Delta R_\lambda = 2\lambda$.) See Figures 18, 19. There is also a secondary lobe close to 60 degrees, which is due to enhancement of contributions from elements on the beam axis. (In this particular computer run the first element in each ring was placed on the beam axis, i.e. $\phi_\ell = \phi_0 = 0$.) It is not exactly at ± 60 degrees because the elements were divided into the total circumference of each ring in an approximate manner and the elements did not line up precisely at 180 degrees from the beam axis. A third enhancement takes place at approximately ± 90 degrees (actual angle varies with element spacing) because here all the elements on the maximum diameters perpendicular to the beam direction are about 2λ apart, and a fourth group of secondary lobes appears at 180 degrees off the beam axis. These four types of sidelobes can all be explained from the above formula, the azimuth angle at which they occur generally increasing as the beam is moving up from horizon. As an example, the same array is shown with the beam pointing at 45 degrees in elevation. (Figure 20, 21)

These four types of secondary lobes are not as strong as the primary beam, of course, because their enhancement is based on a majority group of elements in line with the beam axis and at right angle with the beam axis; in other words, concentration of elements in the areas of the greatest ring diameters. If those groups would deteriorate into two perpendicular linear arrays (e.g. Mills Cross), the echelon lobes would be of the same amplitude as the main beam.

A general increase in backlobes is observed for 1λ element spacing versus 0.25λ , but this has been shown to be a general property of single rings also (see Semi-Annual Report, p. 38) and is independent of the echelon lobe formation.

The elevation patterns of the multi-ring array also show two secondary lobes which exceed the ordinary sidelobe pattern. (See Figures 22, 23) The one at zenith is caused by addition of the contribution from the elements on the (or near the) main beam axis, which are all a full multiple of a wavelength apart, and carry no relative phase when the beam is pointing at horizon. The other, at 60 degrees elevation from horizon, appears because at this angle the path difference

$$d_\lambda = \Delta R_\lambda \cdot \cos \theta$$

is equal to one wavelength.

In an attempt to eliminate all these secondary lobes, elements were arranged in a "star" configuration. This is explained in the next paragraph.

3.2.1.3 Star-Arrays

If elements are arranged so that they have distances smaller than one wavelength between them in the critical areas pointed out above, secondary (echelon) lobes can be avoided. From single-ring investigations it is safe to increase the element spacing within the rings up to about one wavelength, as far as the elevation pattern is concerned, and up to half a wavelength with respect to the azimuth pattern. One possible configuration, leaving the element spacing in radial direction fixed at

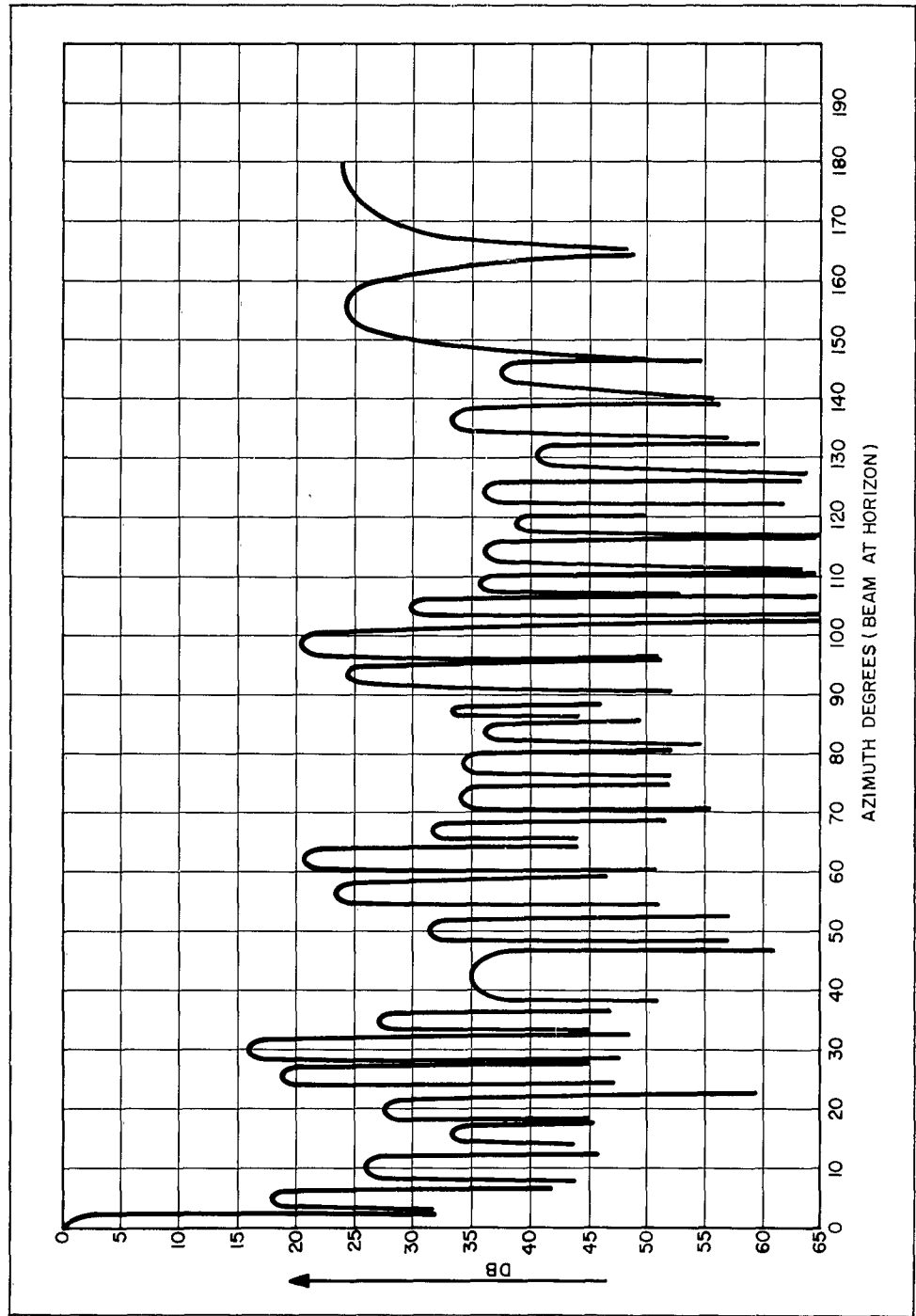


Figure 18. Azimuth Pattern "Multi-Ring Array," 5-Ring Circular Array, $D_{\max} = 20\lambda$,
Element Spacing = 0.25λ , 755 Elements Total

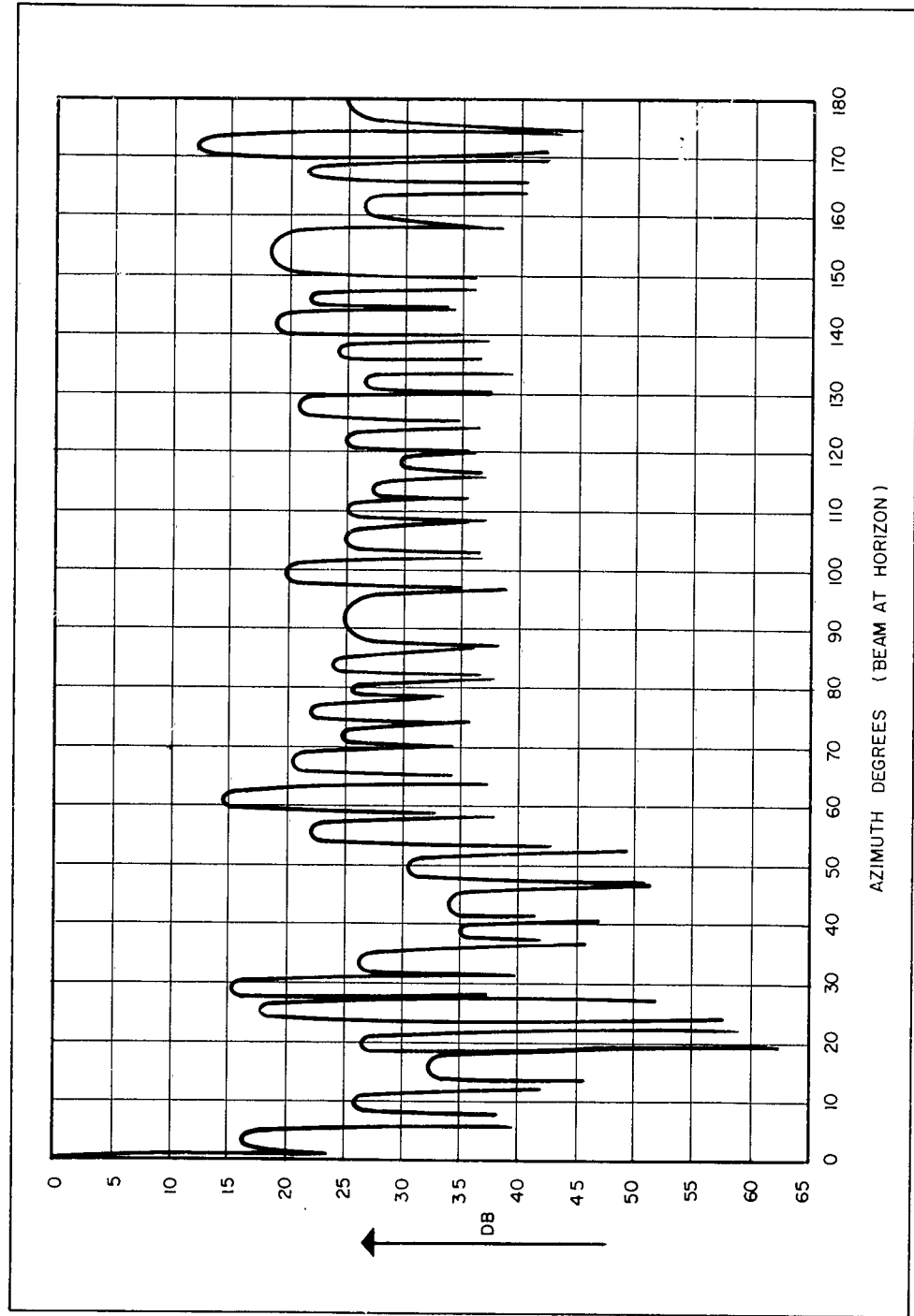


Figure 19. Azimuth Pattern "Multi-Ring Array," 5-Ring Circular Array, $D_{\max} = 20\lambda$,
Element Spacing = 1λ , 139 Elements Total

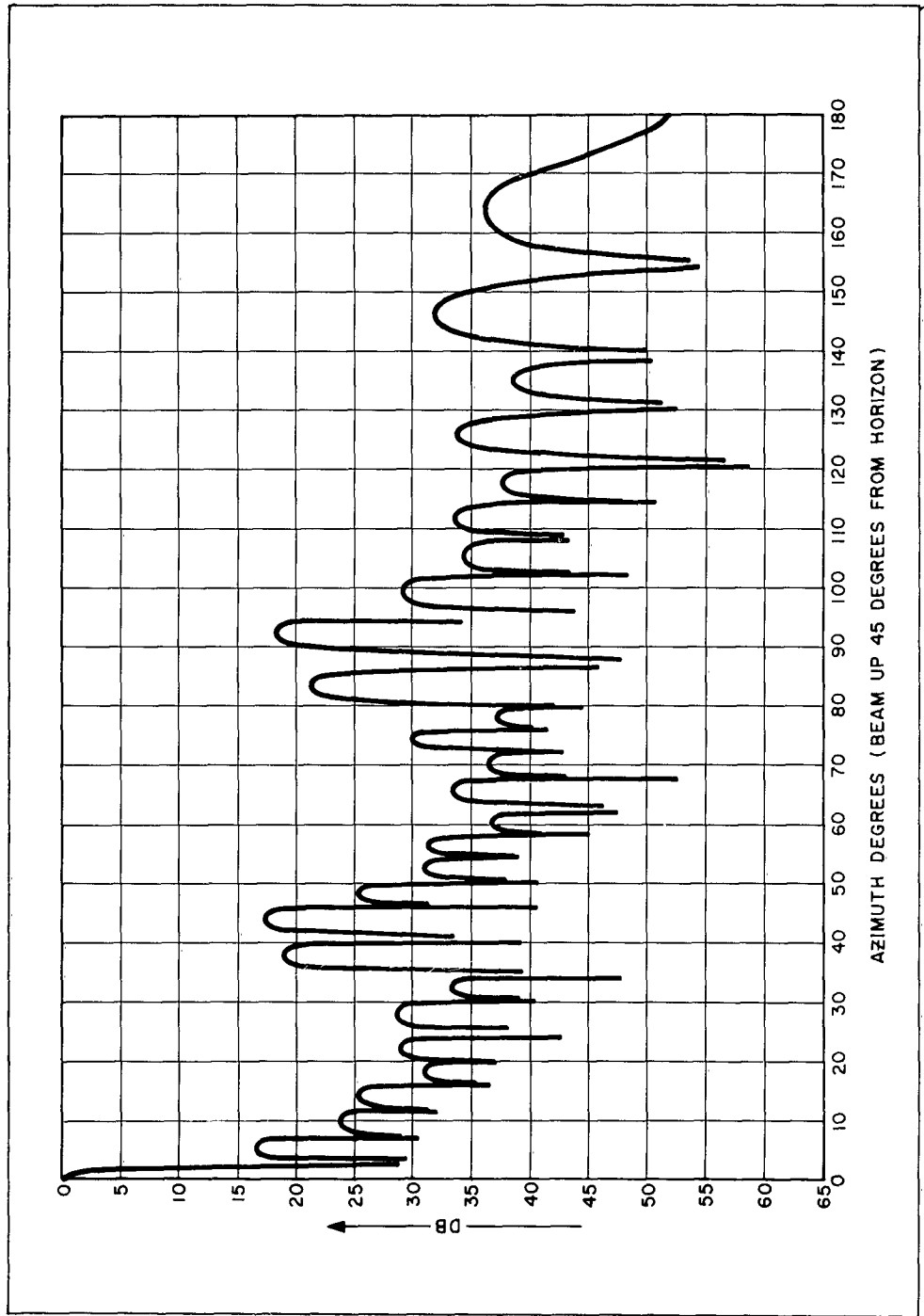


Figure 20. "Multi-Ring Array," 5-Ring Circular Array, $D_{\max} = 20\lambda$, Element Spacing = 0.25λ , 755 Elements Total Azimuth Pattern, Beam Elevated 45°

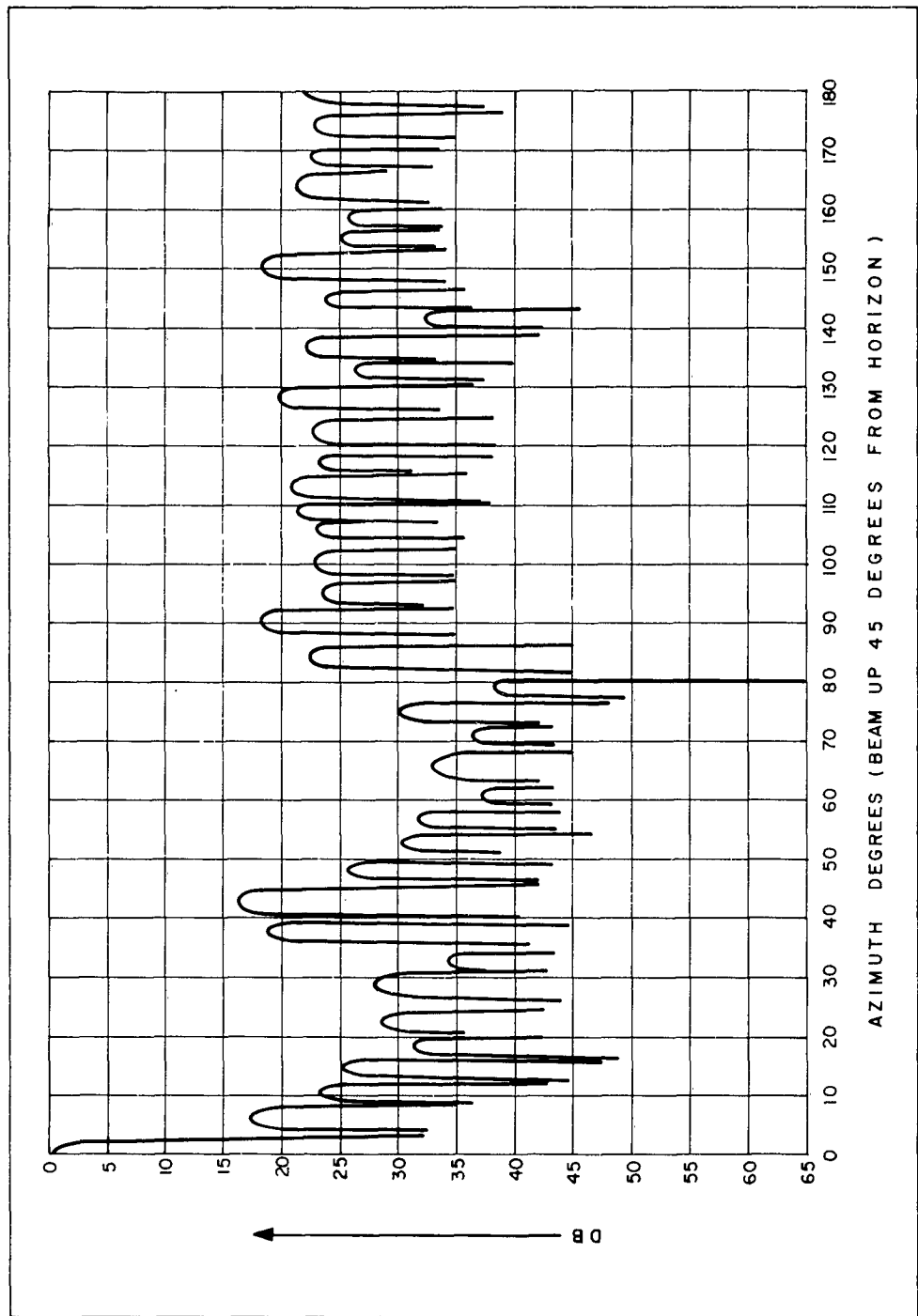


Figure 21. "Multi-Ring Array," 5-Ring Circular Array, $D_{\max} = 20\lambda$, Element Spacing $= 1\lambda$,
188 Elements Total Azimuth Pattern. Beam Elevated 45°

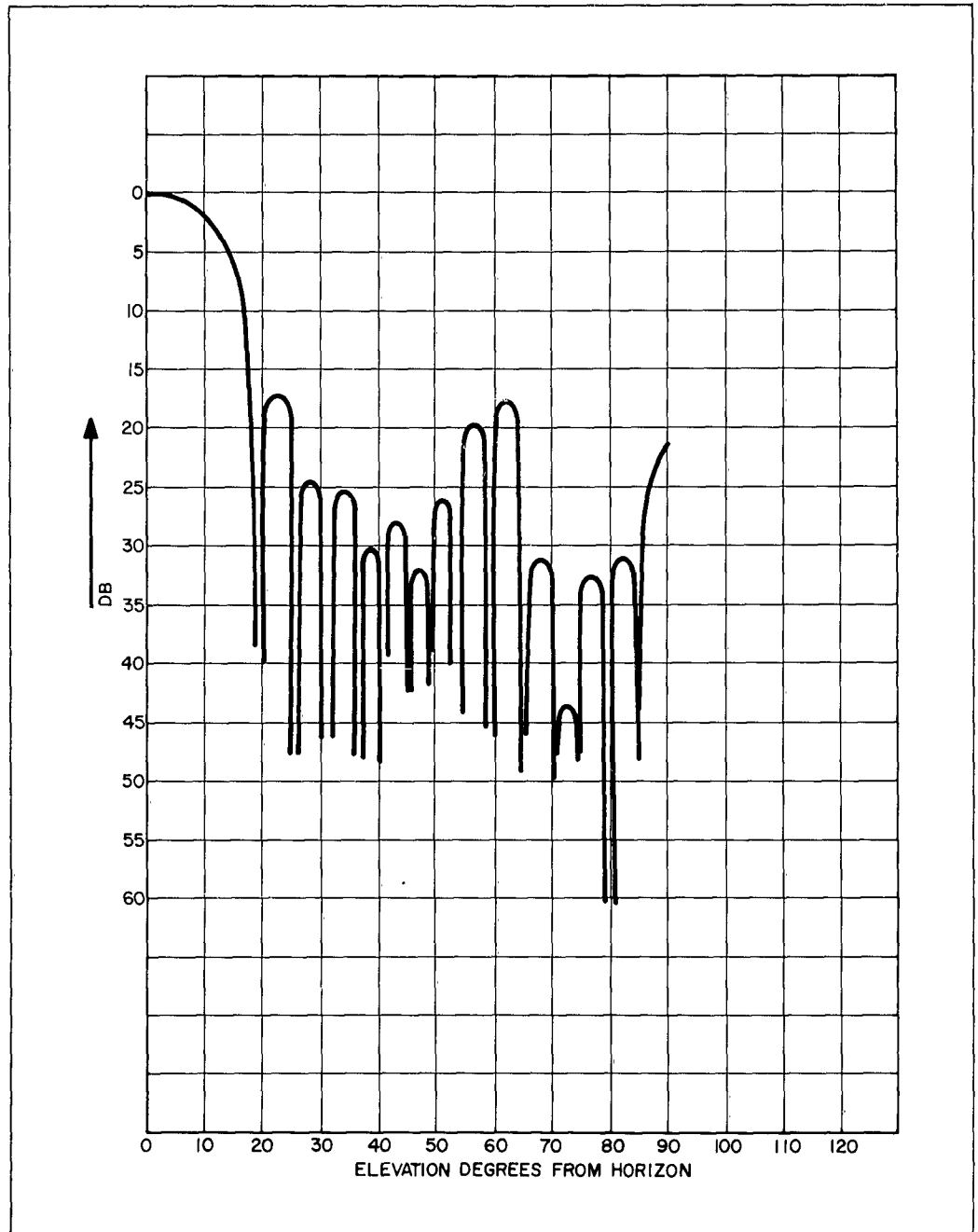


Figure 22. Elevation Pattern "Multi-Ring Array," 5-Ring Circular Array $D_{\max} = 20 \lambda$,
Element Spacing = 0.25λ , 755 Elements Total

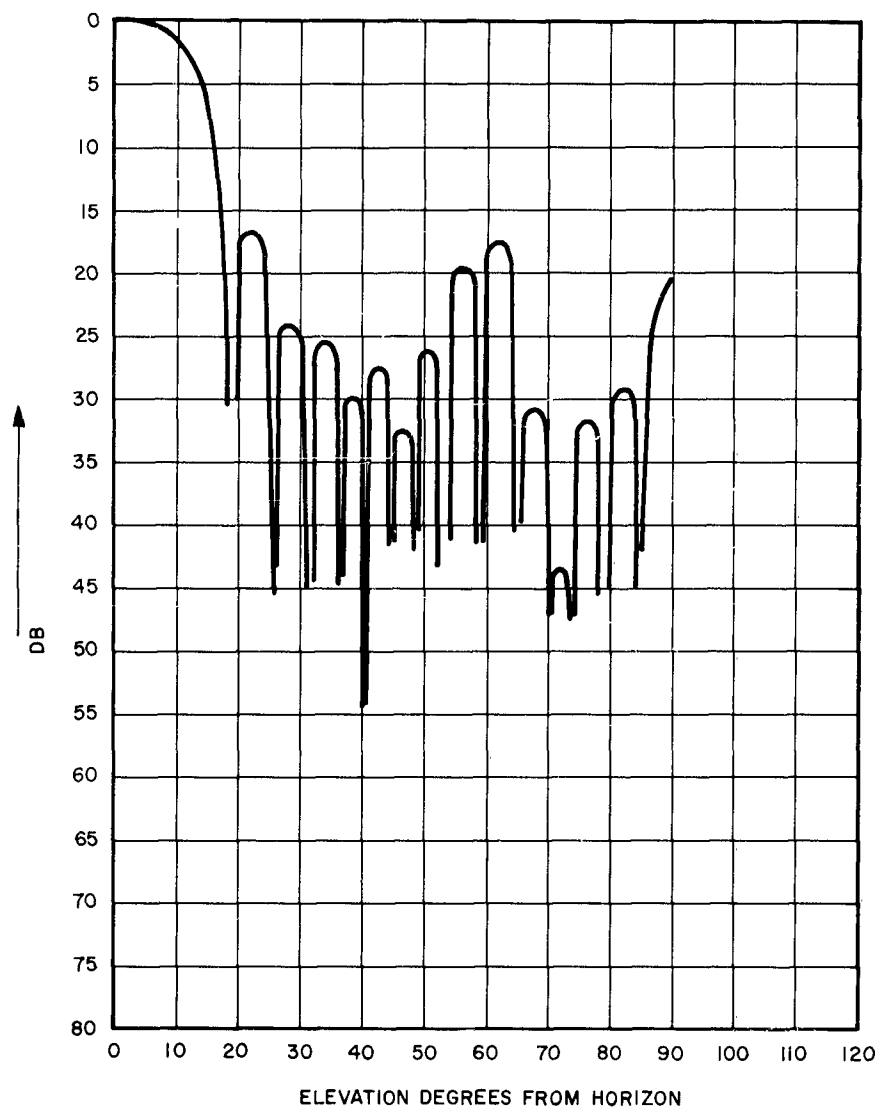


Figure 23. Elevation Pattern "Multi-Ring Array," 5-Ring Circular Array, $D_{\max} = 20\lambda$, Element Spacing = 1λ , 189 Elements Total

half a wavelength and varying it around the circumferences, is shown in Figure 24. Here, the element spacing within the rings varies from a maximum of 1.24λ (ring number 4 from outside) to a minimum of 0.35λ (ring number 10, or innermost ring.)

The resultant patterns show a much greater uniformity of the sidelobe levels (Figures 25 and 26). The total number of elements is greater than in the case of a multi-ring array as described previously, but the star may have to be chosen in cases where the sidelobe requirements do not allow the type of echelon lobe present in the multi-ring array. A comparison of multi-ring and star arrays is shown in tables 1 to 3 listing the sidelobe levels and angles at which they occur* for various element spacings in the ring array and for various thinning techniques within a star array configuration, the difference being in the number of elements per ring and the diameters at which they are thinned out.

3.2.1.4 Conclusions

If echelon lobes of a certain maximum level can be allowed, either because the system requirements are not so much demanding low sidelobes but rather high gain, or because the angular regions in which they occur are being eliminated by the element pattern, then a multiple-ring array, i.e. an array with large spacings in terms of wavelengths between the rings and small spacings within each ring will provide solutions to a given gain requirement which have a minimum number of elements and still have the low first sidelobe (or close to it) characteristic for a continuous circular aperture.

If larger volumes have to be covered, or certain maximum sidelobes have to be observed, either random thinning, or a star-like element configuration can be chosen. The amount of thinning possible again depending on the sidelobe levels that can be tolerated.

3.2.2 MULTI-BEAM OPERATION OF MODULAR CIRCULAR ARRAY

Azimuth beam broadening with a circular array can be achieved by reducing the sector angle of the symmetrical double-arc feed structure. The azimuth beamwidth can thus be increased to about twice the beamwidth of the full ring array without serious degradation of the sidelobe structure. This is achieved by reducing the sector angle to about 45 degrees. For a fixed total number of elements this means that two or more beams can now be radiated simultaneously.

*There are actually more sidelobes than tabulated, and they occur at slightly different angles. However, the sidelobe levels shown are computed maximum values, and there are no sidelobes present which have higher levels.

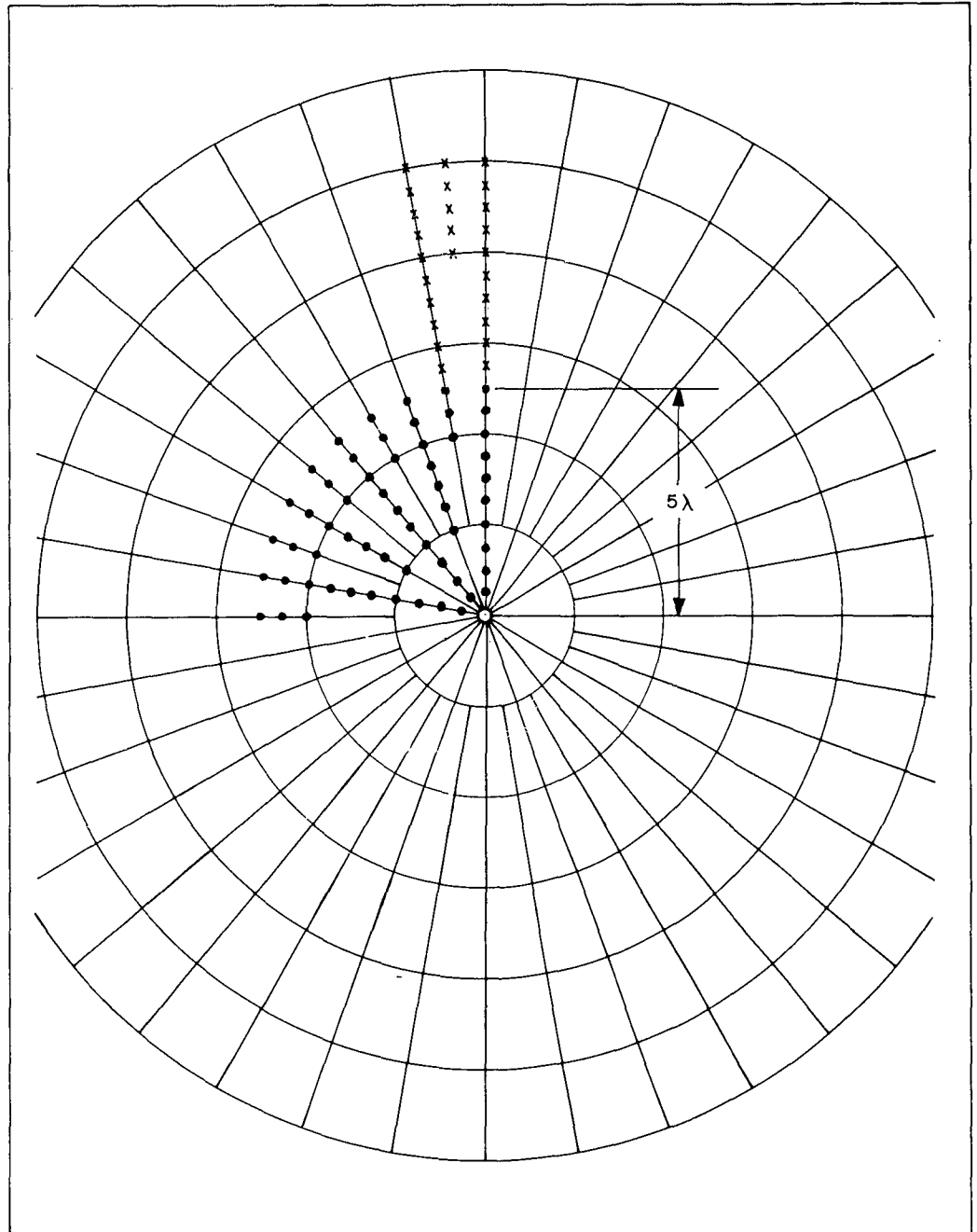
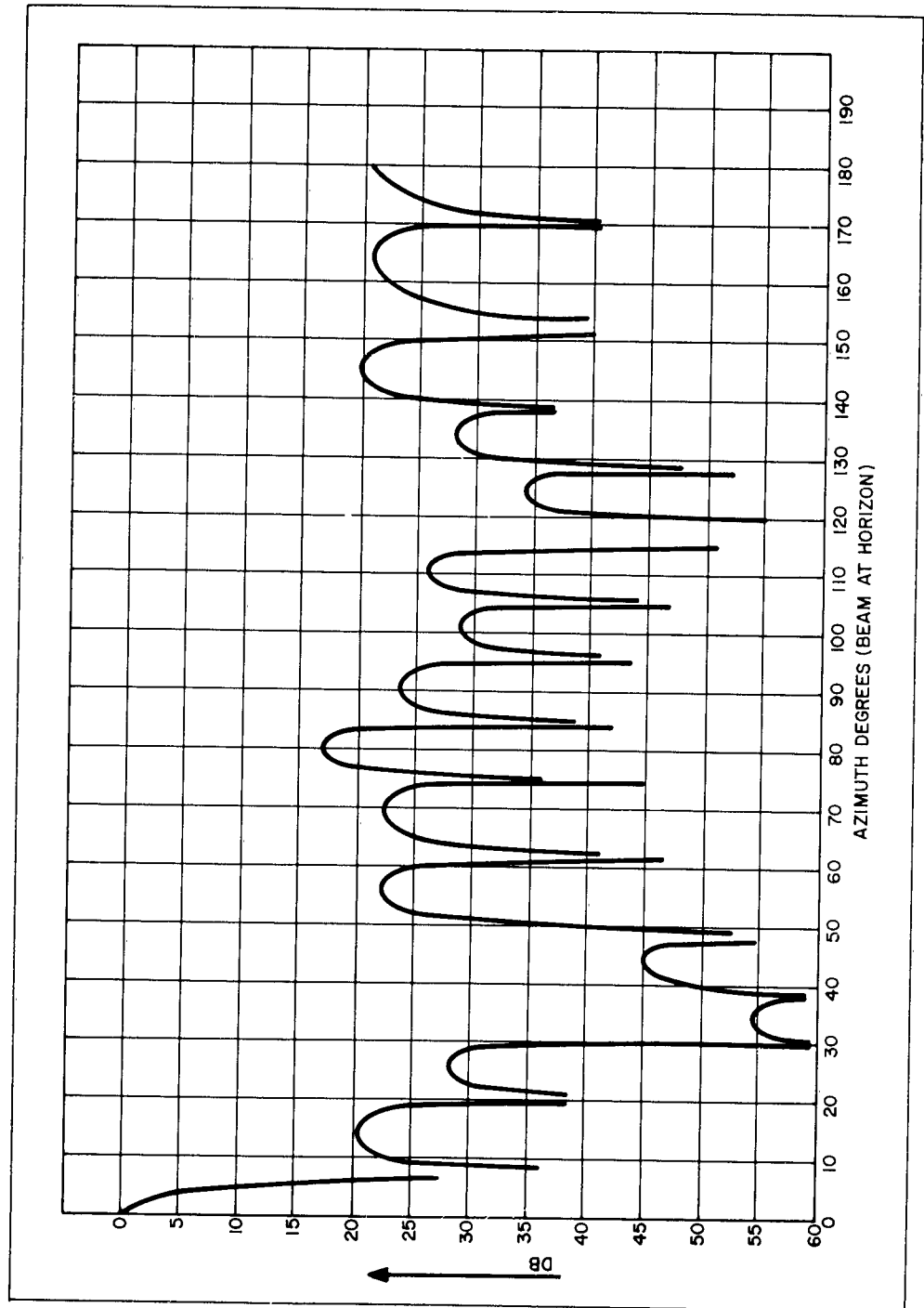


Figure 24. Element Arrangement for One-Quarter of Star Array
Extension to 20λ Diameter Indicated



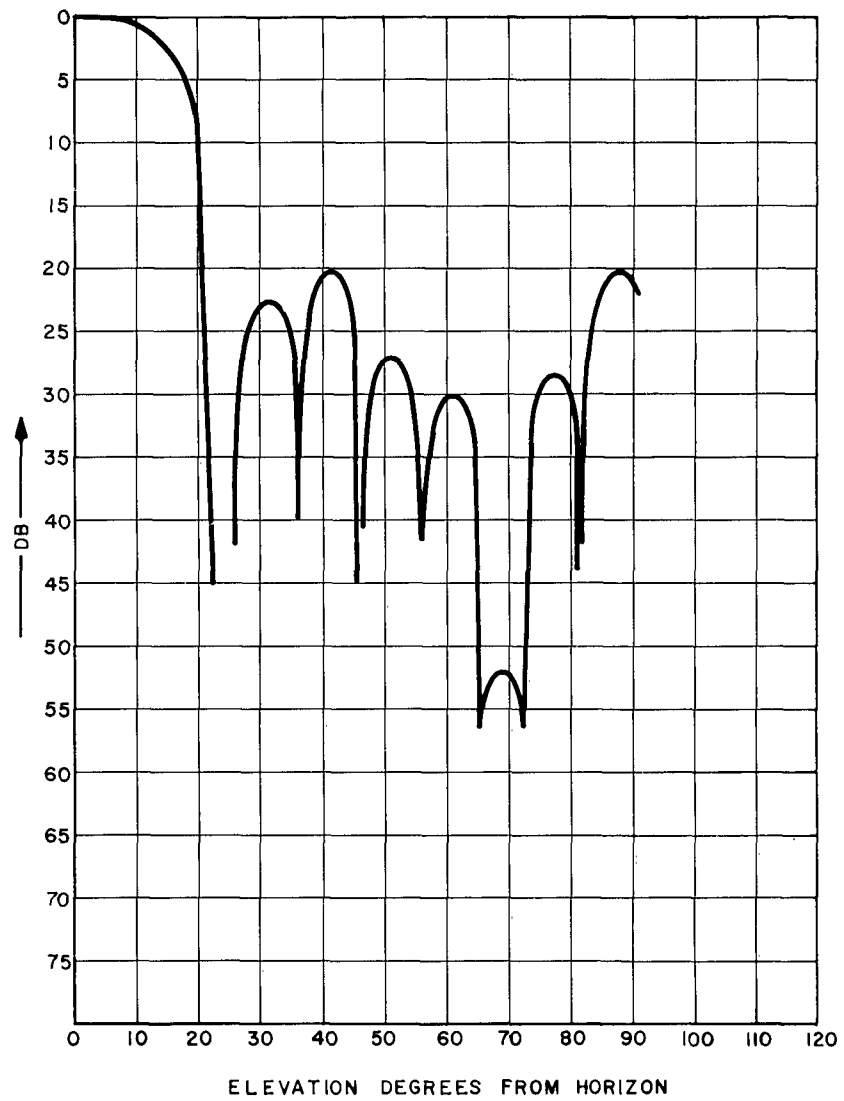


Figure 26. "Star Array," 10-Ring Circular Array, $D_{\max} = 10\lambda$,
Elements Per Ring: 36, 36, 36, 18, 18, 18, 18, 9, 9, 9

TABLE 1
MULTI-RING ARRAY

5 RINGS, CONSTANT SPACING; $D_{\max} = 20\lambda$

S = Element Spacing Within Rings
N = Number of Elements

Sidelobe Levels And Angles At Which They Occur

S = 0.5λ N = 377				S = 0.75λ N = 262			
AZ		ELEV.		AZ		ELEV.	
Angle (deg.)	Level (db)	Angle (deg.)	Level (db)	Angle (deg.)	Level (db)	Angle (deg.)	Level (db)
10°	25.6	22°	16.9	10°	25.5	22°	17
20°	26.8	28°	24.2	20°	26.7	28°	24.2
26°	18	34°	25.2	26°	18	32°	25.1
30°	15.6	38°	30.2	30°	15.6	38°	30.2
34°	26.97	42°	27.9	34°	27.1	42°	27.9
44°	34.90	46°	32.2	40°	35.1	46°	32
50°	31.2	50°	26.3	50°	31.1	50°	26.2
56°	23.4	56°	19.5	56°	23.3	56°	19.5
62°	20.4	62°	17.7	62°	20.4	62°	17.6
66°	31.7	68°	30.9	66°	31.96	68°	31
72°	34.02	76°	32.3	72°	32.9	76°	32.3
78°	34.42	82°	30.6	94°	16.7	82°	30.5
86°	33.5	90°	21	98°	17.9	90°	21.1
94°	24.24			104°	24.2		
98°	20.58			110°	24.98		
104°	29.7			116°	17.1		
108°	35.62			124°	19.5		
124°	34.4			138°	21.9		
130°	36.4			146°	22.3		
136°	30.4			150°	21.9		
144°	29.3			158°	23.8		
152°	20.9			164°	23.8		
158°	24.85			168°	25.8		
162°	21.2			176°	18.4		
166°	23.95						
172°	18.2						
176°	21.6						

TABLE 2
MULTI-RING ARRAY

5 RINGS, CONSTANT SPACING; $D_{\max} = 20\lambda$

S = Element Spacing Within Rings
N = Number of Elements

Sidelobe Levels And Angles At Which They Occur

S = 2λ N = 95				S = 5λ N = 39			
AZ		ELEV.		AZ		ELEV.	
Angle (deg.)	Level (db)	Angle (deg.)	Level (db)	Angle (deg.)	Level (db)	Angle (deg.)	Level (db)
10°	25.4	24°	16.8	14°	11.2	22°	17.5
20°	28	30°	24.6	20°	17.7	28°	23.1
26°	19.1	36°	24.8	24°	16.3	40°	9.7
34°	14.1	40°	29.9	30°	25.4	50°	13.8
42°	21.5	44°	27.5	36°	15.2	56°	10.6
46°	18.9	48°	32.9	42°	15.1	62°	13.96
52°	18	52°	24.7	48°	18.2	66°	11.7
60°	13.6	58°	18.5	52°	22.2	70°	11.1
70°	18.4	64°	12.1	56°	17.7	78°	13.2
76°	19.96	72°	13.3	60°	13.3	86°	7.4
82°	19.2	80°	18.1	64°	15.5		
90°	20.2	84°	22.1	68°	18.5		
94°	15.9	88°	19.6	76°	18.97		
102°	16.9			84°	18.7		
106°	21.8			90°	10.8		
110°	20.7			96°	15.5		
122°	19.7			100°	13.8		
130°	21.4			108°	17		
134°	17.9			114°	14.97		
140°	16.5			124°	8.5		
146°	17.6			134°	23.1		
150°	17.6			140°	16.3		
160°	22			144°	17.5		
166°	25.5			152°	11.3		
174°	16.2			162°	12.97		
180°	17.98			172°	7.99		

TABLE 3
"STAR ARRAY"

10 RING, VARIABLE ELEMENT SPACING; $D_{\max} = 10\lambda$

N = Number Of Elements

Sidelobe Levels And Angles At Which They Occur

N = 300				N = 225				N = 207			
AZ		ELEV.		AZ		ELEV.		AZ		ELEV.	
Angle (deg.)	Level (db)	Angle (deg.)	Level (db)	Angle (deg.)	Level (db)	Angle (deg.)	Level (db)	Angle (deg.)	Level (db)	Angle (deg.)	Level (db)
15°	19.5	40°	19.4	15°	19.5	40°	21.4	15°	20.3	40°	21.2
25°	28.7	55°	29.0	25°	31.0	55°	31.3	55°	22.1	85°	20.4
35°	46.2	75°	35.7	45°	39.6	70°	34.5	70°	21.7		
45°	37.8	90°	23.0	60°	21.3	90°	21.3	80°	16.5		
60°	23.0			70°	24.9			90°	23.3		
85°	21.6			85°	20.6			110°	25.5		
110°	22.7			95°	34.3			145°	19.7		
135°	21.7			110°	20.98			165°	20.98		
150°	25.8			135°	22.5			180°	20.4		
170°	17.4			150°	21.5						
180°	17.7			170°	19.0						
				180°	15.97						

3.2.2.1 Beams At Right Angles

The maximum sector angle at which two beams can be generated (in a double arc array) is $\alpha = 90$ degrees. The two beams are then at right angles to each other (Figure 27a).

This configuration provides two beams of about 16 to 20 degrees width in azimuth, with backlobes in the order of -10 db. The total system gain is better than 12 db because we have two beams of better than 15 db gain each. Since in the 48-element array the element positions are fixed, and 2^n ($n = 1, 2, 3, 4$) elements per arc are desirable for a binary symmetrical feed, 8 elements per arc are selected with a sector angle of 52.5 degrees (Figure 27b). This gives added protection against beam interference and mutual coupling between elements at the extreme edges of the arcs. The azimuth beamwidth is about 23 degrees, and the gain of an azimuth beam of this

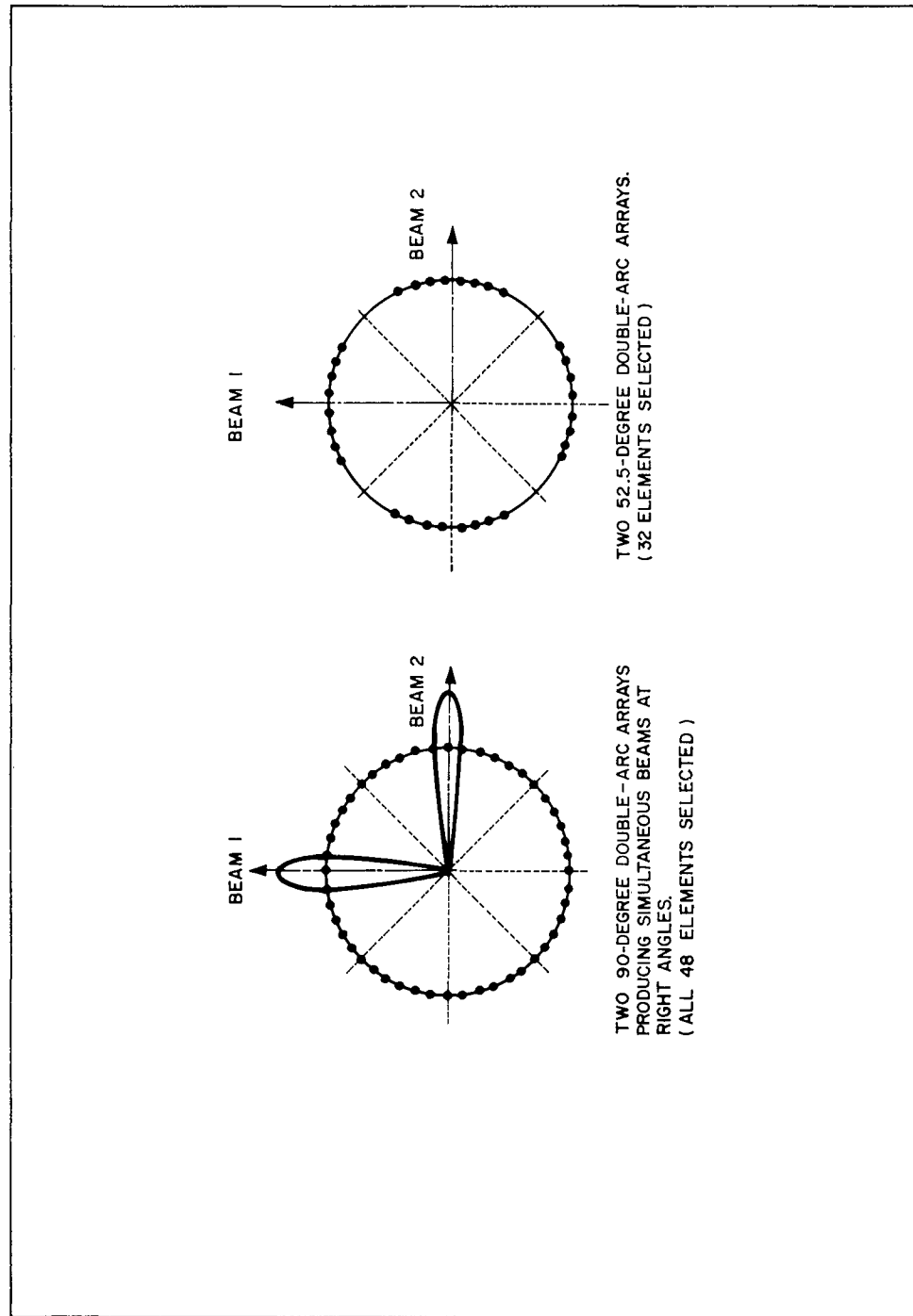


Figure 27. Double Arc Arrays Producing Beams at Right Angle

width was calculated to be about 15 db for an elevation beamwidth of 24 degrees. Since the actual elevation beamwidth of the 52.5-degree double arc is only 21 degrees, the gain should be accordingly better.

The total system gain for two beams is thus 12 db. The beams can, in addition, be squinted relative to each other by ± 7.5 degrees in azimuth (the available angular increment in element spacing) without any change in mutual coupling effects, and by ± 15 degrees with only a slight increase in mutuals. (The actual effects are complex because they do not only involve change in impedance matching due to mutual impedances, but also interference of the beams. They have to be investigated experimentally.)

If all available elements were utilized for beam squinting, then the relative beam positions could be varied as much as ± 30 degrees, thus providing coverage (center beam positions) from 60 degrees to 120 degrees, relative to the center of the other beam, in steps of 7.5 degrees for the beam maximum.

However, when the maximum variation is used, the edge elements of the two beams are only 0.26λ apart, and strong interference due to mutual coupling is bound to occur. The result of this interference may bring up the null between the two beams, but it could also result in a strongly increased backlobe. Therefore, this extreme operation should be avoided and relative beam positions other than $90^\circ \pm 15^\circ$ should be attempted by other means.

If now four arcs were phased so that they radiate as single-arc arrays, we get four beams with a theoretical overall gain of 9 db (Figure 28a). Also, if two arcs are grouped together to form a single beam and the other two are used to form two separate beams, we have triple beam operation with a theoretical overall gain of 10.2 db (Figure 28b).

In actuality the gain will be much less for the single arc configuration because of the large increase in elevation beamwidth (for 82.5 - degree single arcs the elevation beamwidth is 64 degrees vs. 22 for the double arc) so that the element pattern determines the gain in elevation. Besides, for the 82.5-degree single arc several of the sidelobes in azimuth are only 7.5 db. For better sidelobes the arc has to be either larger ($>120^\circ$) or smaller ($<55^\circ$), thus indicating a "forbidden region". For the smaller sector angles the gain reduction is so severe that it is better to use an omnidirectional mode. The larger sector angles limit the amount of beam squinting possible with a double-beam single-arc array. All beams can be rotated around, of course, only the relative beam positions being fixed.

3.2.2.2 Beams At Arbitrary Angles

It was already pointed out in the previous section that small variations in relative beam position are possible. If larger deviations from the right-angle condition are desired, the following two solutions avail themselves:

- a) the use of still smaller sector angles, with an increase in backlobe level to a point where we have bi-directional operation,
- b) the use of single arcs.

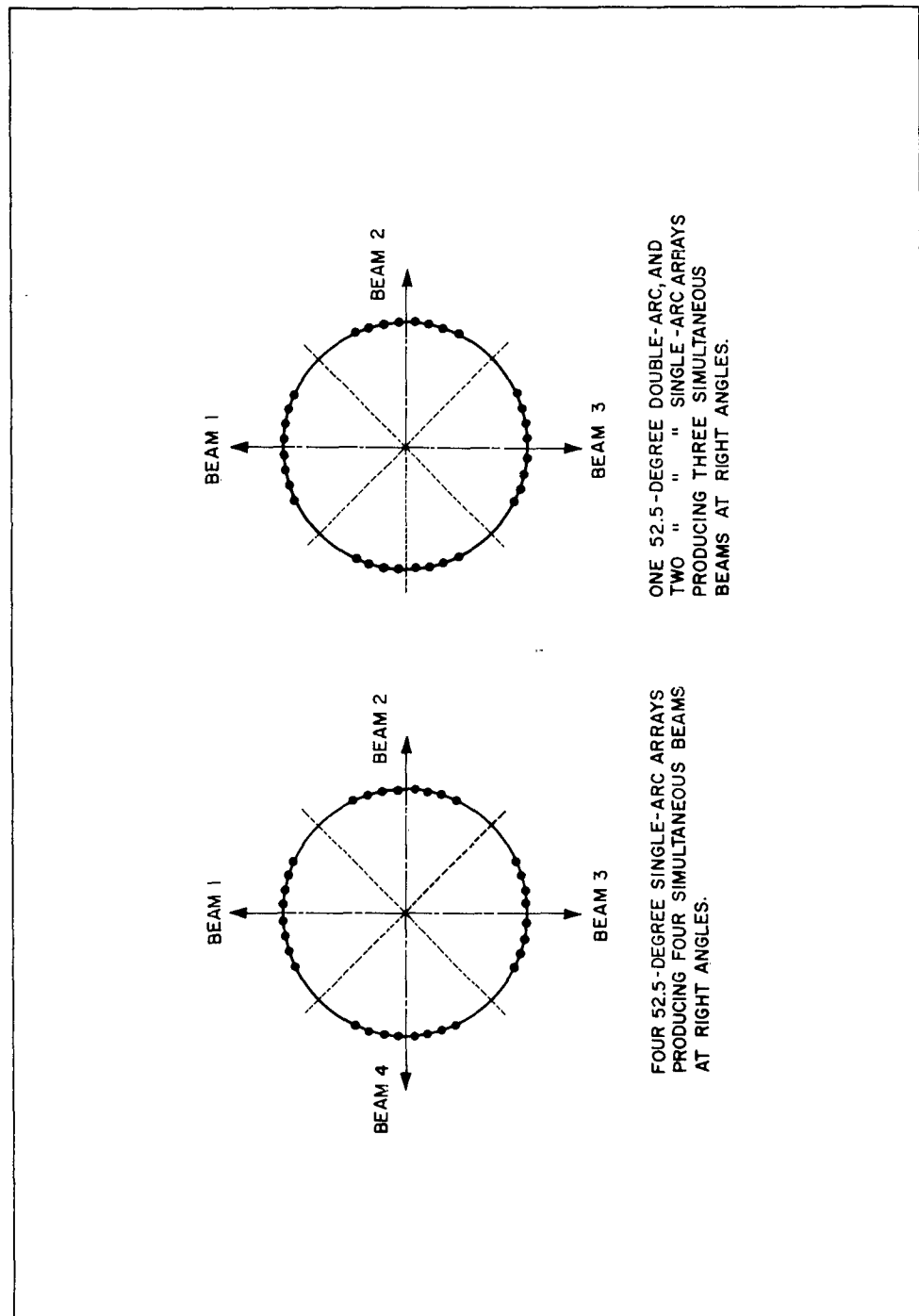


Figure 28. Modular Ring Arrays Producing Three and Four Beams

a) In the case of a 22.5-degree double-arc array, we have a backlobe of 28 degrees beamwidth (in azimuth) which is down 0.5 db from the main lobe, and a main lobe beamwidth of 35.6 degrees. These are the values for uniform amplitude distribution. With an amplitude weight on the elements (e.g., 30-db Tchebycheff taper), the backlobe could be brought up to the same level as the main lobe, and the beamwidth could be further increased. Since only eight elements are involved in the total array, a number of these double-arc feeds could be placed around the ring to point beams in practically any direction. Beam overlap at the 3 db-points is possible for two adjoining double-arc arrays with a sector angle $\alpha < 30^\circ$ (Figure 29). The system gain in this case would be better than 9 db, because for decreasing sector angle the elevation beamwidth also decreases, thus over-compensating for the increase in elevation sidelobe level, provided we have a dipole (monopole) element pattern.

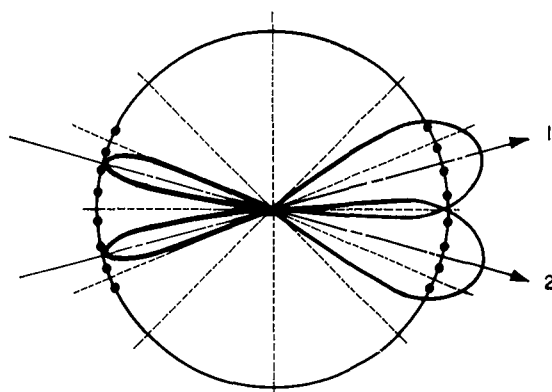
b) A single-arc array has higher sidelobes in azimuth and only one broad beam in elevation. To stay within a reasonable limit for the azimuth sidelobe levels (≈ -10 db), the sector angle has to be 120 degrees or more. This limits this type of array to two beams with relative positions from 120 degrees (two adjoining arcs) to 180 degrees (back to back), or three beams with fixed 120 degree relative beam position (Figure 30). The three-beam case is undesirable both from the standpoint of mutual coupling and gain.

3.2.2.3 Summary of Multi-Beam Modular Array

In the following chart a comparison is made between the various beam directions which can be selected simultaneously, the angular ranges covered by the specific beams, the approximate gain associated with the theoretical antenna system and the amount of difficulty expected when implementing the operational parameters into a practical antenna structure.

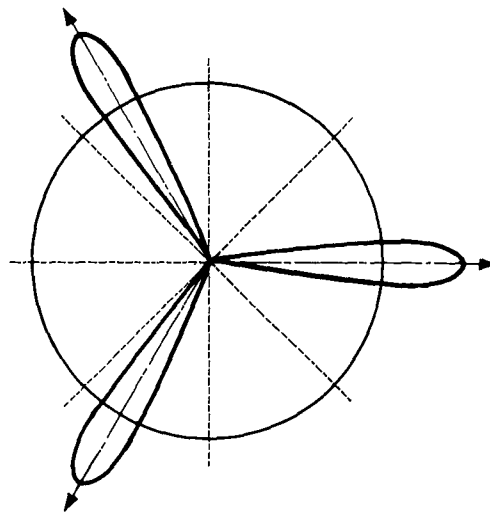
In conclusion, it should be remarked that the same array (provided broadband antenna elements are used) can be built for a range of frequencies, with according change in beamwidth and gain, if so desired. The feed networks would have to be exchanged, however, unless broadband phase shifters (e.g. ferrite phasers) and power dividers have been employed.

Also, higher gains will be possible if the diameter of the array is increased.



48-ELEMENT CIRCULAR ARRAY.
16 ELEMENTS SELECTED IN TWO
ADJOINING 22.5-DEGREE DOUBLE-ARC
ARRAYS WITH OVERLAPPING
FORWARD BEAMS.

Figure 29. 48 Element Circular Array: Forming Two Overlapped Forward Beams



48-ELEMENT CIRCULAR ARRAY.
48 ELEMENTS SELECTED IN THREE
120-DEGREE SINGLE-ARC ARRAYS.

Figure 30. 48 Element Circular Array: Pattern for Three Single-Arc Feeds



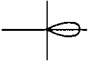

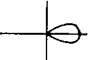
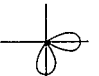
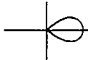
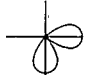
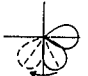
Type of Feed	Beamwidth (Deg.))		Max. Sidelobe (DB))		Gain (DB)	Max. Relative Angular Azimuth Range (Deg.)	Rel. Beam Center (Deg.)	Max. Contin Azimuth Ra (Deg.)	
	AZ	EL	AZ	EL					
I <u>Full Ring</u> 1) OmniDirectional	360	11,5	-	-	6	-180 to + 180	0	360	
	2) Directional	10 to 12	24	-7,9 to -11 -11 to -8	18	-6 to +6	0	12	
II <u>120-Degree Single Arc</u> 1) Single Beam	13	60	-10	-	13	-6,5 to + 6,5	0	13	
	2) Double Beam	13	60	-10	-	10	173,5 ± 60 to 186,5 ± 60	180 ± 60	13
III <u>82,5-Degree Double Arc</u> 1) Single Beam	16 to 20	22	-8,6 to -10,3	-4 to -3,4	16	-10 to + 10	0	20	
	2) Double Beam	16 to 20	22	-8,6 to -10,3	-4 to -3,4	13	-10 to + 10 and 80 to 100	0 90	20
IV <u>52,5-Degree Double Arc</u> 1) Single Beam	23	21	-9,2	-3,5	15	-11,5 to + 11,5	0	23	
	2) Double Beam a) Right	23	21	-9,2	-3,5	12	-11,5 to + 11,5 78,5 to 101,5	0 90	23
	b) Arbitrary Angles	23	21	-9,2	-3,5	12	-11,5 to + 11,5 78,5 ± 30 to 101,5 ± 30	0 90 ± 30	23

*) Single Values For Constant Amplitude Weight; If Two Values Are Given, The First Is For Constant Weight, The Second For 27-db Tchebycheff.

**) Degree of Difficulty In Increasing Order.



CHART 1
 $D = 4\lambda$, $\Delta\phi = 7.5^\circ$, $\Delta S = 0.262\lambda$
 $\lambda/4$ - MONOPOLE ELEVATION PATTERN

	Beamwidth (Deg.) *)		Max. Sidelobe (DB) *)		Gain (DB)	Max. Relative Angular Azimuth Range (Deg.)	Rel. Beam Center (Deg.)	Max. Continuous Azimuth Range (Deg.)	Mutual Coupling **)	Shape of Composite Pattern (Without Sidelobes)
	AZ	EL	AZ	EL						
	360	11.5	-	-	6	-180 to +180	0	360	0	
	10 to 12	24	-7.9 to -11	-11 to -8	18	-6 to +6	0	12	1	
Arc	13	60	-10	-	13	-6.5 to +6.5	0	13	1	
	13	60	-10	-	10	173.5 ± 60 to 186.5 ± 60	180 ± 60	13	2 to 4	
Arc	16 to 20	22	-8.6 to -10.3	-4 to -3.4	16	-10 to +10	0	20	1	
	16 to 20	22	-8.6 to -10.3	-4 to -3.4	13	-10 to +10 and 80 to 100	0 90	20	2	
Arc	23	21	-9.2	-3.5	15	-11.5 to +11.5	0	23	1	
	23	21	-9.2	-3.5	12	-11.5 to +11.5 78.5 to 101.5	0 90	23	1	
	23	21	-9.2	-3.5	12	-11.5 to +11.5 78.5 to 30 to 101.5 ± 30	0 90 ± 30	23	1 to 3	

Constant Amplitude Weight; If Two Values Are Given, The
 First Is For 20-db Tchebycheff, The Second For 27-db Tchebycheff.

Increasing Order.



Type of Feed	Beamwidth (Deg.) *)		Max. Sidelobe (DB) *)		Gain (DB)	Max. Relative Angular Azimuth Range (Deg.)	Rel. Beam Center (Deg.)
	AZ	EL	AZ	EL			
V 22.5-Degree Double Arc							
1) Double Beam *)	36 + 28	20.5	-8	-3	12.8	-18 to + 18 166 to 194	0 180
2) Quadruple Beam							
a) Beam at Rt. Angle	36 + 28	20.5	-8	-3	9	-18 to + 18 72 to 108 166 to 194 256 to 284	0, 90 180, 270
b) Arbitrary Beam Angle	36 + 28	20.5	-8	-3	9	-18 to + 18 72 ± 60 to 108 ± 60 166 to 194 256 ± 60 to 284 ± 60	0, 90 ± 60 180, 270 ± 60
VI Combinations							
52.5 Degree and 22.5 Degree Double Arcs							
a) Beams at Rt. Angles	23 36 + 28	21 20.5	-9.2 -8	-3.5 -3.0	11	-11.5 to + 11.5 72 to 108 166 to 194	0, 90 180
b) Arbitrary Beam Angles	23 36 + 28	21 20.5	-9.2 -8	-3.9 -3.0	11	-11.5 to + 11.5 72 ± 45 to 108 ± 45 166 ± 45 to 194 ± 45	0, 90 ± 45 180 ± 45

*) Backlobe Down 0.5 DB For Constant Amplitude Weight.
Backlobe Beamwidth = 28 Deg.



CHART 1 (Continued)
 48 - ELEMENT MODULAR CIRCULAR ARRAY
 $D = 4\lambda$, $\Delta\phi = 7.5^\circ$, $\Delta S = 0.262\lambda$
 $\lambda/4$ - MONOPOLE ELEVATION PATTERN

	Beamwidth (Deg.) *)		Max. Sidelobe (DB) *)		Gain (DB)	Max. Relative Angular Azimuth Range (Deg.)	Rel. Beam Center (Deg.)	Max. Continuous Azimuth Range (Deg.)	Mutual Coupling **)	Shape of Composite Pattern (Without Sidelobes)
	AZ	EL	AZ	EL						
Beam Arc *)	36 + 28	20.5	-8	-3	12.8	-18 to +18 166 to 194	0 180	36	1	
Beam t, Angle	36 + 28	20.5	-8	-3	9	-18 to +18 72 to 108 166 to 194 256 to 284	0, 90 180, 270	36	2	
Beam	36 + 28	20.5	-8	-3	9	-18 to +18 72 ± 60 to 108 ± 60 166 to 194 256 ± 60 to 284 ± 60	0, 90 ± 60 180, 270 ± 60	36 (72)	2 to 4	
Beam Arcs t, Angles	23 36 + 28	21 20.5	-9.2 -8	-3.5 -3.0	11	-11.5 to +11.5 72 to 108 166 to 194	0, 90 180	36	2	
Beam	23 36 + 28	21 20.5	-9.2 -8	-3.9 -3.0	11	-11.5 to +11.5 72 ± 45 to 108 ± 45 166 ± 45 to 194 ± 45	0, 90 ± 45 180 ± 45	36	2 to 4	

*) DB For Constant Amplitude Weight,
 th = 28 Deg.

3.2.2.4 Experimental Results

Figures 31 and 32 shows the experimental model of a single ring array of 32 radiators. The model frequency was about 2000 MC. Both directional and omnidirectional patterns were tested, but the results were not too good because of the large amount of reflections in the small laboratory test space.

An omnidirectional feed arrangement corresponding to a J_8 -elevation pattern showed a maximum variation of ± 3 db over 360 degrees in azimuth. The elevation pattern at the same time had a 40-degree beamwidth, and about a -12 db first sidelobe. Beam maximum was at zero elevation. When 4 elements were fed in a single arc, a beamwidth of about 21 degrees was measured, and first sidelobes were about 16 db down from the main beam. The azimuth beamwidth was narrower than should be expected, probably because of parasitic excitation of the adjacent elements. More accurate tests were not made because of the high cost of the necessary power dividers and phase shifters. Only 3 power dividers had been purchased, and phasing was accomplished by inserting proper lengths of coaxial transmission line. Since the elements (for the omnidirectional case) were paired without impedance matching, the different lengths of transmission line resulted in different amount of impedance transformation and had undoubtedly the effect of different currents on the radiators.

If, in the future, more accurate tests would be run, all these factors would have to be taken into consideration. At present, unfortunately, the conclusions that can be drawn from these tests are fairly limited. However, except for the effects of mutual coupling, which are also covered in Sections 3.2.1 and 3.3, the theoretical conclusions on ring arrays are certainly valid because they are based on vector addition of the isotropic element contributions, and not on approximations.

3.2.3 PATTERN OF A MULTI-RING ARRAY OF ISOTROPIC SOURCES FROM SUPERPOSITION OF THE CONTRIBUTIONS OF THE INDIVIDUAL ELEMENTS.

3.2.3.1 Plane Ring Array

The summation of the contributions of all elements in the case of a plane ring array leads to the following general equation.

$$E(\theta, \phi) = \sum_{m=1}^M \sum_{\ell=1}^{L_m} A_m \exp j \left\{ \psi_{\ell m} - \frac{2\pi r}{\lambda} \sin \theta \cos(\phi - \phi_{\ell m}) \right\} \quad (1)$$

here $\psi_{\ell m}$ is the phase of the illumination of element ℓ on ring m

$\phi_{\ell m}$ = azimuth angle of element ℓ on ring m

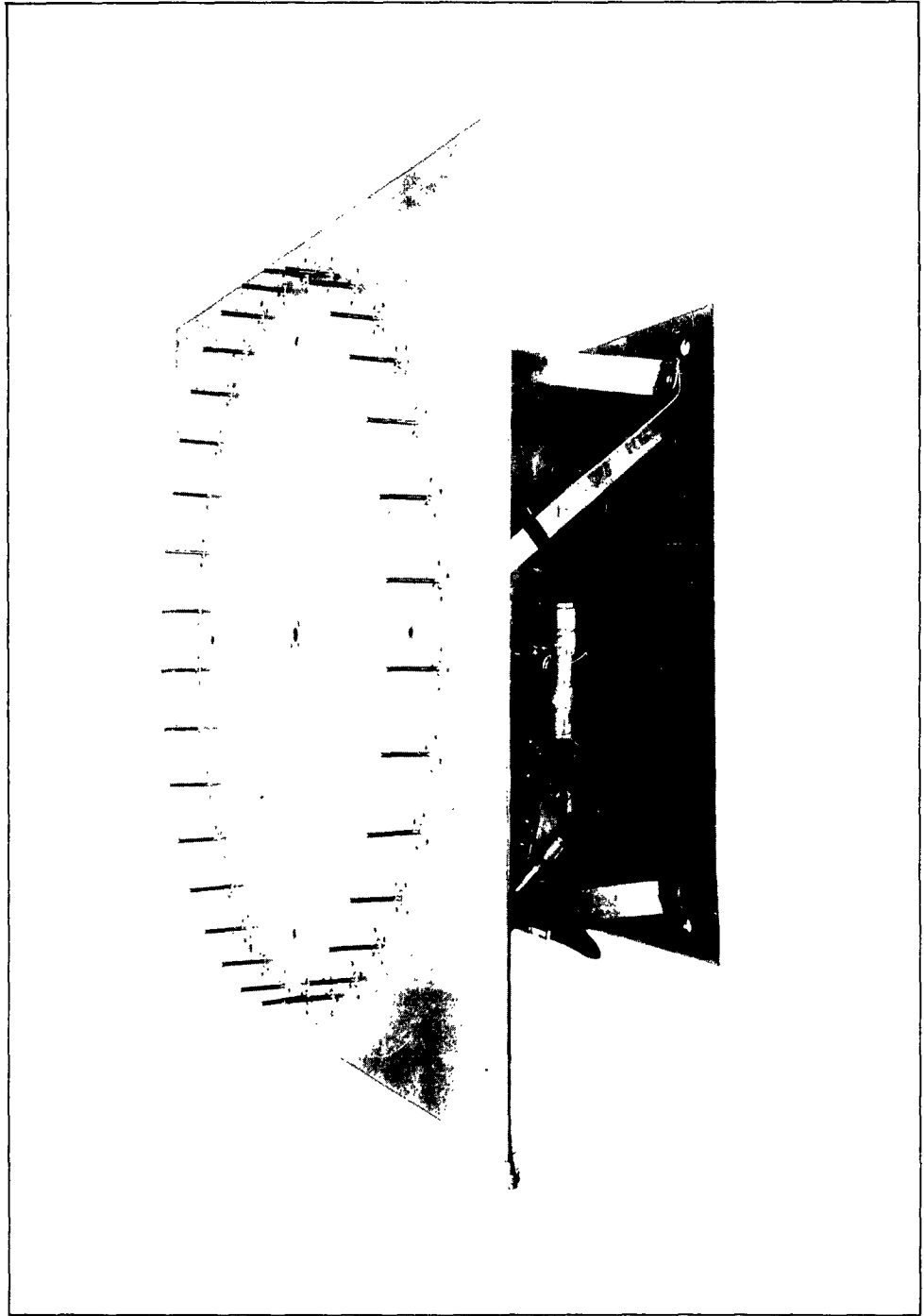


Figure 31. Experimental Model: Top View

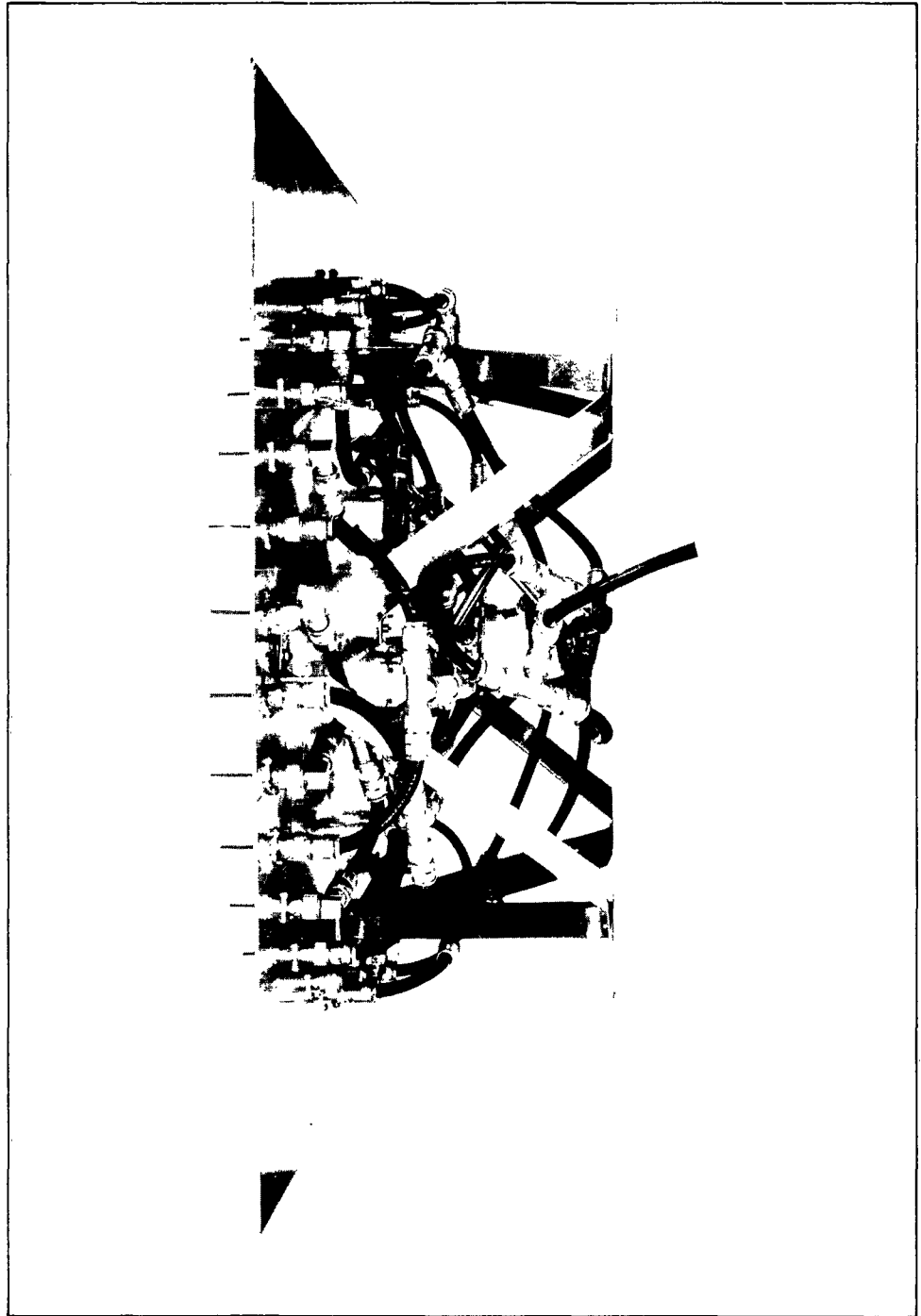


Figure 32. Experimental Model: Bottom View

If we make

$$\psi_{\ell m} = \frac{2\pi r_m}{\lambda} \sin \theta_{om} \cos (\phi_{om} - \phi_{\ell m}) \quad (2)$$

then the array pattern has its maximum value for $\theta = \theta_{om}$, $\phi = \phi_{om}$ and the pattern equation is

$$E(\theta, \phi) = \sum_{m=1}^M \sum_{\ell=1}^{L_m} A_m \exp j \left\{ \frac{2\pi r_m}{\lambda} \left[\sin \theta_{om} \cos (\phi_{om} - \phi_{\ell m}) - \sin \theta \cos (\phi - \phi_{\ell m}) \right] \right\} \quad (3)$$

where θ_{om} , ϕ_{om} are the angles of the beam maximum for ring m

$$L_m = \text{total number of elements on ring m}$$

3.2.3.2 Generalized Array With Arbitrary Ring Envelope

If all rings are horizontal and concentric, but are not located in one plane, we can write the formula in the following way:

$$E(\theta, \phi) = \sum_{m=1}^M \sum_{\ell=1}^{L_m} A_m \exp j \left\{ \delta_{\ell m} - \frac{2\pi d}{\lambda} \ell m \right\} \quad (4)$$

where A_m = Amplitude of m_{th} ring, $A \neq f(\phi)$

$$d_{\ell m} = r_m \left[\cos \theta_m \cdot \cos \theta \cdot \cos (\phi - \phi_{\ell m}) + \sin \theta_m \sin \phi \right] \quad (5)$$

$$\text{with } \phi_{\ell m} = \frac{2\pi}{\lambda} \cdot \ell \pm \phi_{\ell m o} \quad (6)$$

and $\phi_{\ell m o}$ = angular displacement of first element ($\ell = 1$) on each ring with respect to main beam direction

$$\delta_{\ell m} = \frac{2\pi}{\lambda} d_{\ell m} (\theta_o, \phi_o), \text{ where } \theta_o, \phi_o = \text{angles of main beam} \quad (7)$$

θ_m = angle of envelope of ring array with horizon at the point where the envelope touches ring m as shown in Figure 33.

In order to facilitate multiple pattern investigations on a digital computer, the pattern equation is now re-written for relative power:

$$P(\theta, \phi) = \left[\sum_{m=1}^M \sum_{\ell=1}^{L_m} A_m \cos \left(\delta_{\ell m} - \frac{2\pi}{\lambda} d_{\ell m} \right) \right]^2 + \left[\sum_{m=1}^M \sum_{\ell=1}^{L_m} A_m \sin \left(\delta_{\ell m} - \frac{2\pi}{\lambda} d_{\ell m} \right) \right]^2 \quad (8)$$

for $\theta = \theta_o, \phi = \phi_o$ we get:

$$P(\theta_o, \phi_o) = P_o = \left[\sum_{m=1}^M \sum_{\ell=1}^{L_m} A_m \right]^2 \quad (9)$$

And the normalized pattern equation is:

$$P^*(\theta, \phi) = \frac{1}{P_o} \cdot P(\theta, \phi) \text{ where } P_{\max}^* = P^*(\theta_o, \phi_o) = 1 \quad (10)$$

The actual far-field pattern of the array can then be found by taking the square root of the values in the power pattern above (Formula 8). and multiplying the resulting gain pattern by the element pattern of the chosen antenna element.

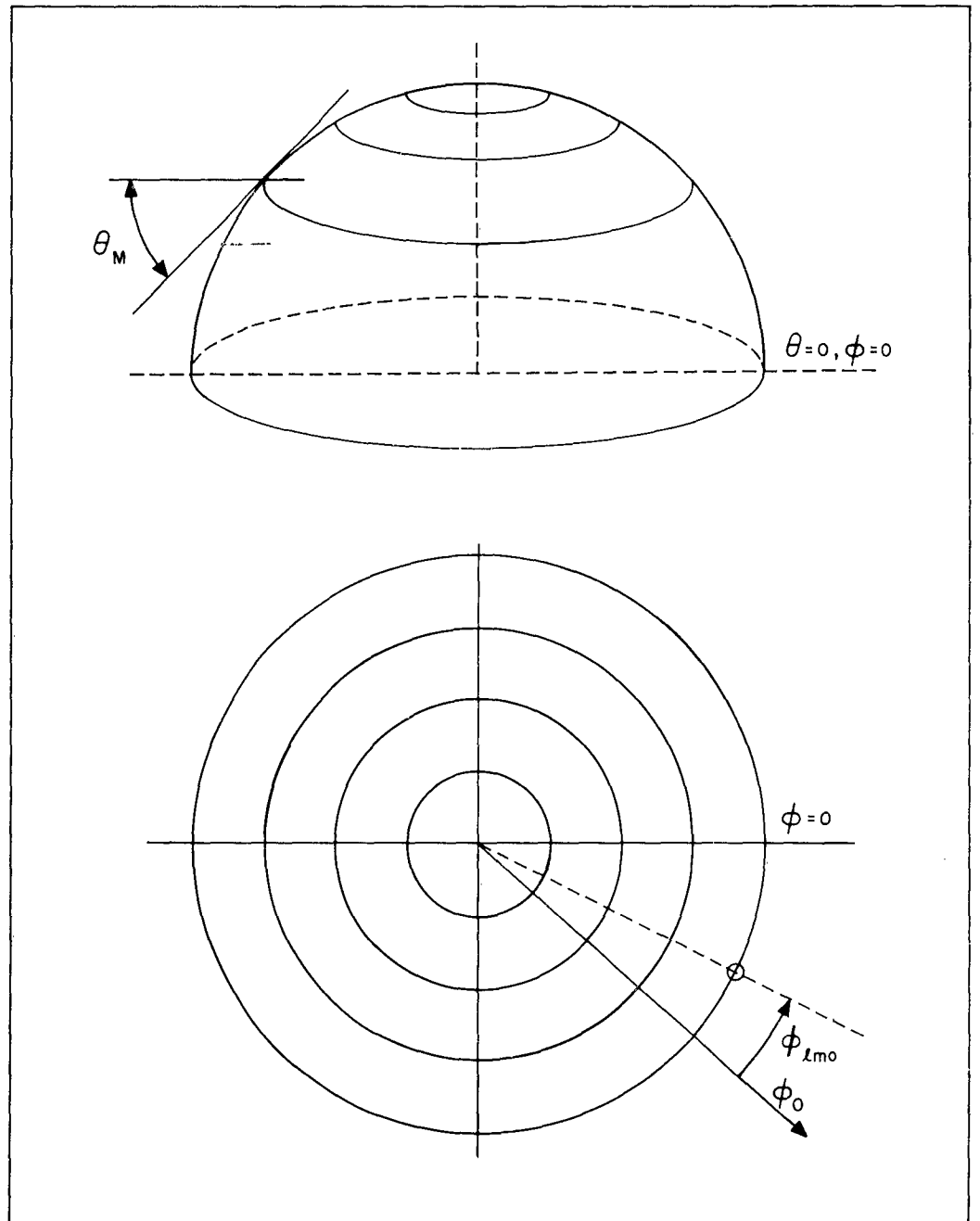


Figure 33. Volumetric Coverage of Ring Array

3.2.4 OPERATIONAL PROBLEMS OF CIRCULAR ARRAYS WITH MAXIMUM RADIATION NEAR HORIZON

3.2.4.1 Electronic Scanning Over Limited Angular Range

The beam of the circular array configurations discussed in the previous chapters can be steered electronically (in addition to simple mechanical rotation of the feed) over a limited angular range, either by adjusting the phase of each element by means of switched digital phasers, with the minimum phase increment dictated by the minimum phase change required for the elements closest to the beam axis for a given increment of beam direction, or with continuously variable phasers, such as ferrite phase shifters. The phase change for a desired change in beam direction, as a function of the element position, is given by (See Figure 34):

$$\Delta \psi = 360 R_{\lambda} \left\{ \cos [\phi_e - (\phi_o + \Delta \phi_o)] - \cos [\phi_e - \phi_o] \right\}$$

where ϕ_o = original beam direction

$\Delta \phi_o$ = scanning angle

ϕ_e = element angle with respect to original beam direction

R_{λ} = radius of array in wavelengths

If we now let ϕ_o be the reference, or $\phi_o = 0$, we get

$$\Delta \psi = 360 R_{\lambda} \left\{ \cos [\phi_e - \Delta \phi_o] - \cos \phi_e \right\}$$

The phase differential required for beam steering is thus clearly a function of element position.

For $\phi_e = 0^\circ$; we get

$$\begin{aligned} \Delta \psi &= 360 R_{\lambda} [\cos (-\Delta \phi_o) - 1] \\ &= -720 R_{\lambda} \sin^2 \frac{\Delta \phi_o}{2} \end{aligned}$$

For $\phi_e = 90^\circ$

$$\begin{aligned} \Delta \psi &= 360 R_{\lambda} [\cos (90 - \Delta \phi_o) - 0] \\ &= 360 R_{\lambda} [1 - \cos \Delta \phi_o] \\ \Delta \psi &= 360 R_{\lambda} [1 - \cos \Delta \phi_o] \\ &= 720 R_{\lambda} \sin^2 \frac{\Delta \phi_o}{2} \end{aligned}$$

This means that the phase increment for the elements close to the original beam direction is an order of magnitude smaller than the phase differential for the elements at right angles to the beam direction. Therefore, the minimum increment in beam direction is determined by the minimum increment in phase for the elements close to the beam axis. This corresponds to the odd linear phase slope required for scanning a linear broadside array.

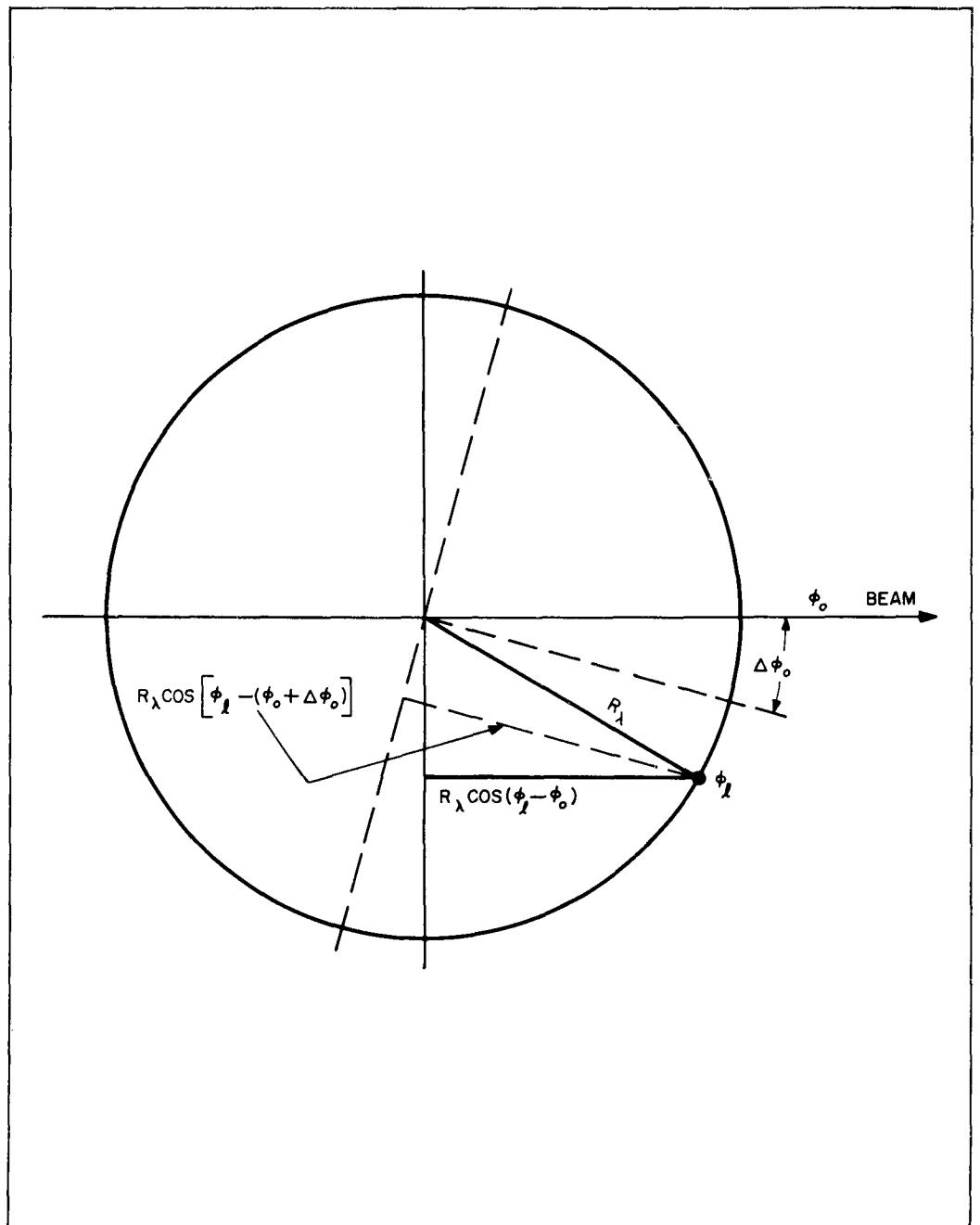


Figure 34. Change of Element Phase with Beam Direction

3.2.4.2 Effect Of Phase Errors

3.2.4.2.1 Systematic Errors

Because of the properties of the phase differential as discussed above, it is not very likely that a phase contour around the circumference would develop, due to phase errors in the elements, which has the exact behavior for a certain beam increment $\pm \Delta \phi_0$.

For instance, if the same type and model phase shifter were used throughout the system, and if a sudden drop or rise in temperature would occur, or a sudden increase or decrease in modulation voltage, all elements would experience the same phase error, and no beam pointing error would develop.

In the case of a double-arc array, as the sector angle gets small, we can write the change in beam direction as

$$\Delta \phi_0 = \pm \arccos \left\{ 1 - \frac{|\Delta \psi|}{360 R_\lambda} \right\}$$

In the case of 4λ - diameter array, and assuming a phase error of ± 7.2 degrees, we find that $\arccos 0.99 = 8.1$ degrees. Since the beamwidth approaches 46.2° as the sector angle $\alpha \rightarrow 0$, *) the relative change in beam position is, even if we assume that the phase error has opposite sign for the elements opposite each other, not very critical. For overlapping beams, however, the region of overlap should be large enough to provide coverage even under adverse phasing conditions.

3.2.4.2.2 Random Phase Errors

If we had random fluctuations in the element phasing, such as caused by limited reproducibility of the phase adjustment in motor-tuned mechanical phasers, then we would get **)

$$\delta \phi_0 = \frac{2\Delta \phi_0 \cdot \delta \psi_e}{\left\{ 2 N_e \right\}^{\frac{1}{2}}}$$

where $\delta \phi_0$ is the standard deviation of the beam angle, $\delta \psi_e$ the standard deviation of the element phasing, and N_e the effective number of elements.

3.2.4.3 Effects of Ground Conditions On Element Pattern

So far it has been assumed that the $\frac{\lambda}{4}$ - monopoles are used for elements in the circular array. The data for gain and elevation beamwidth as compiled under "Multi-Beam Operation" have as a prerequisite perfect image formation for all angles of incidence of a wavefront, including grazing incidence. Perfect image formation, however, is only guaranteed if a perfectly conducting infinite ground plane is present. For any deviation of the ground conductivity from the

*) See First Semi-Annual Report, Page C-6

**) Private Communication From S. Applebaum

infinitely conducting case there will be considerable deterioration of the elevation pattern near the grazing angle. If a metal ground plane is used for mounting the elements, the critical angle at which element pattern deterioration starts because of insufficient image formation is given by

$$\alpha \text{ crit} = \arctan \frac{h}{r}$$

where h = height of element over ground plane,

r = radius of ground plane.

For instance, if a radius-over-height ratio of 100 were used ($h = \frac{\lambda}{4}$; $D = 50\lambda$), the critical angle is $\alpha \text{ crit} \approx 0.6$ degrees.

A metal ground plane would provide good image formation up to X - band and beyond *), but the size of the plane appears prohibitively large for frequencies below 1000 MC, even if only a wire grid were used. The surrounding soil, which is not useful for image formation at X - band, becomes more and more effective as the frequency is decreased. This is so because the conductivity, and the resultant reflection coefficient, is highly frequency dependent for frequencies above 2 GC. Below 2 GC, however, the conductivity of water is fairly constant with frequency, and only a function of electrolytic dissociation. Now the complex permittivity can be calculated as

$$\begin{aligned} \epsilon^* &= \epsilon_r - j 60 \delta \lambda \\ &= \epsilon_r - j 18,000 \frac{\delta}{f} \end{aligned}$$

where ϵ_r is the relative permittivity,

δ the conductivity in Mhos per meter,

λ the wavelength in meters,

f the frequency in megacycles.

Table I shows the relative permittivity and the conductivity of various media, as well as the complex permittivity for $f = 300$ MC.

*) JOHNK, ASTIA AD 245 033

TABLE I

Material	Relative Permittivity	Conductivity	$\epsilon^* = n^2$
Sea Water	80	1	80 - 60j
Fresh Water	80	10^{-3}	80 - 0.06j
Wet Loam	24	0.6	24 - 36j
Dry Loam	2	3×10^{-2}	80 - 1.8j
Wet Farm Soil	20 to 40	10^{-1} to 10^{-2}	(20 40) - (6 0.6)j
Dry Farm Soil, Sand	4 to 10	10^{-2} to 10^{-4}	(4 10) - (0.6 0.006)j
Pastures	10 to 15	5×10^{-4}	(10 15) - 0.03j
Light Forest	10	1.5×10^{-4}	10 - 0.009j
Rocks, Mountains	4 to 10	10^{-3}	(4 10) - 0.06j
Frozen Ground	3 to 4	10^{-5}	(3 4) - 0.0006j

Table II shows various arbitrary complex permittivities, and the conductivities required to achieve them as a function of frequency, with the minimum elevation angle for which the elevation pattern has not decreased more than 10 db from the maximum value.

TABLE II

n^2	$= 5 \times 10^{-4}$ Mhos/meter	5×10^{-3}	5×10^{-2}	5×10^{-1}	α Min
7 - 0.3j	30 MC	300	3,000	-	4°
7 - 3j	3	30	300	3,000	4°
7 - 30j	0.3	3	30	300	2.5°
7 - 300j	0.03	0.3	3	30	1°
7 - ∞	Infinite metal ground plane				0

It is apparent that even with optimum ground conditions (seawater), only poor radiation can be expected at grazing incidence. A good metal ground plane is, therefore, imperative for good radiation in the horizontal plane, except for very low frequencies.

Alternate solutions to the problem are: to provide each radiating element with a ground plane of its own, which is tilted down, or to tilt the element itself into a conical shape. The first solution results in the so-called "Discone" antenna, the other in the conical monopole (Figures 35a and 35b). Both types have structural problems, especially with respect to the feed. A modification of the discone, the top-loaded folded monopole with conical ground plane, would result in good structural stability, but no data is available (Figure 35c).

For very low frequencies even relatively poor ground conditions have little effect on the element pattern. Here, the size of the ground plane is determined by the ohmic losses in the transition regions between the antenna and the surrounding medium. The ground plane has to be large enough to reduce the currents to a safe level.

3.2.4.4 Pattern Deterioration In The Far Field

Regardless of the element pattern's quality, in the regions far away from antenna there will be attenuation of the electromagnetic wave propagating close to the ground due to the ground losses.

Again, only for long and very long waves the attenuation is negligible, so that a ground wave can propagate. (Figure 36).

The conditions can be improved by providing an artificial medium far enough away from the antenna, so that attenuation of the ground wave does not start, before the major portion of the radiated energy is far enough away from the ground (for higher frequencies with quasi-optical propagation) due to the earth's curvature for minimum loss. This could be accomplished, for instance, by means of an artificial lake or canal in the direction (or directions) of desired propagation. By the same token, missing good ground conditions could be used for additional sidelobe suppression in undersirable directions (Figure 37).

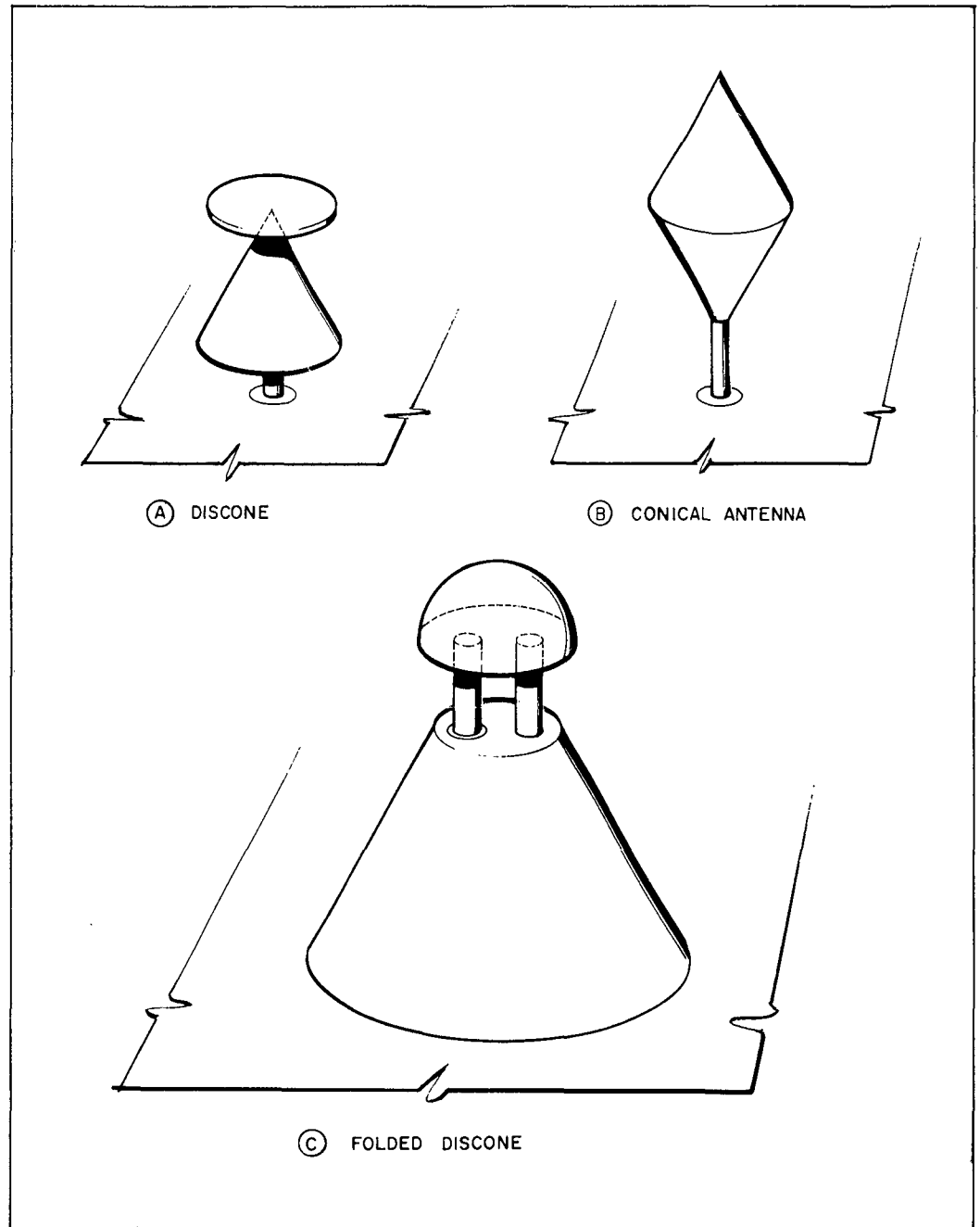


Figure 35. Individual Element Ground Plane Variations

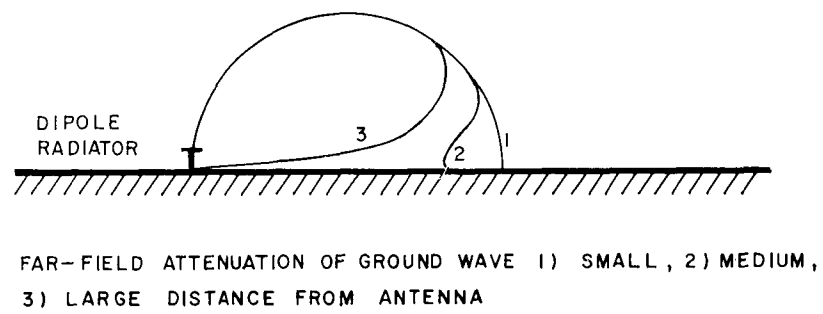


Figure 36. Attenuation of Propagated Wave Due to Ground Losses

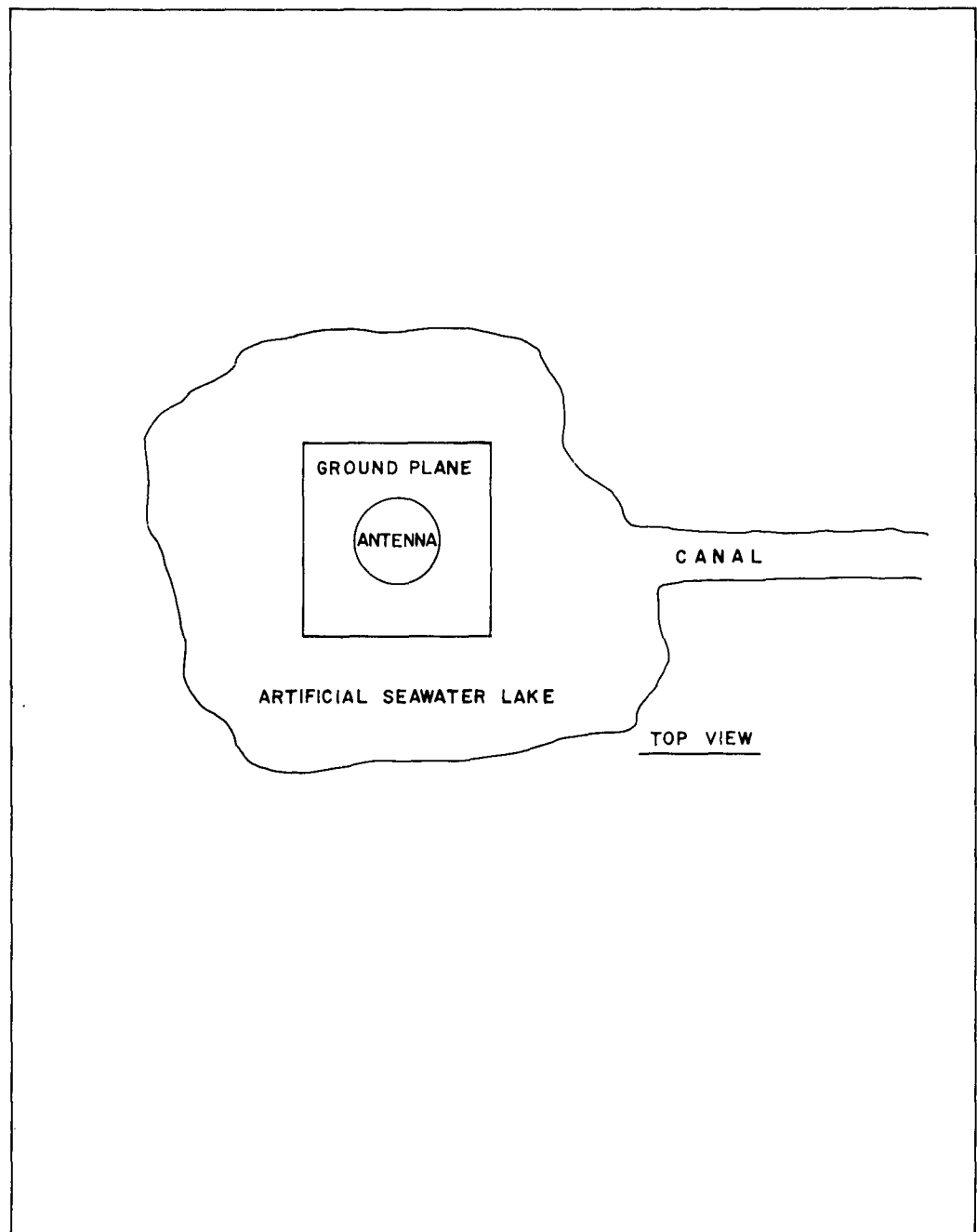


Figure 37. Ground Wave Propagation Improvement With Artificial Lake

3.3 The Use of Scattering Matrices in the Measurement of Mutual Coupling

To study the effects of mutual coupling a mathematical approach as one would find in Radiation Lab Series #10 becomes too complicated for general use. Some means should be devised so that a complete picture of mutual coupling can be shown. For example, an analysis that separately treats the effects of terminal matching of the antenna, power radiated and power coupled to the adjacent antenna, would be useful.

A scattering matrix approach to mutual coupling was considered because scattering parameters are closely associated with power transfer properties of a network, and they exist for every physical passive networks. It should be noted that there is not an impedance or admittance matrix for every passive network. Furthermore, the impedance scheme fails to give a complete detailed account of network operation since it is based on the linear fractional transformation of a single complex variable which is taken to represent the ratio of a complex voltage to a complex current rather than the transformation of voltage and current themselves.

The scattering matrix approach is a middle course between two unsatisfactory extremes, one the complicated step of solving field equations and the other an over-simplified equivalent circuit approach.

A lossy microwave transmission two-port junction would appear as shown below:



In the complex plane the reflection coefficient as seen at terminal one (Γ) can be expressed as a function of the reflection coefficient at terminal 2 (Γ').

$$\Gamma = \frac{A\Gamma' + B}{C\Gamma' + D}$$

Proof of this relationship was performed by William Altar on the basis of one mode electromagnetic field theory. By use of Maxwell-field equations he showed that the cross ratios of the reflection coefficient remain invariant when transmitted through a microwave passive junction.

$$R(\Gamma, \Gamma_1; \Gamma_2, \Gamma_3) = R(\Gamma', \Gamma'_1; \Gamma'_2, \Gamma'_3)$$

or

$$\frac{(\Gamma - \Gamma_2)(\Gamma_1 - \Gamma_3)}{(\Gamma - \Gamma_3)(\Gamma_1 - \Gamma_2)} = \frac{(\Gamma' - \Gamma'_2)(\Gamma'_1 - \Gamma'_3)}{(\Gamma' - \Gamma'_3)(\Gamma'_1 - \Gamma'_2)}$$

which leads to

$$\Gamma = \frac{A\Gamma' + B}{C\Gamma' + D}$$

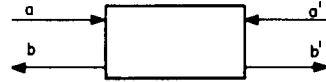
This bilinear transformation appears very simple; however, it is very deceiving because it is performed in the complex plane. The transformation was shown to be true for lossy passive networks in references (2), (3) and (4). They presented a method, called the sliding short method, whereby the transmission and reflection parameters in phase as well as magnitude could be read directly from a Smith Chart. An outline of the sliding short method is given in Section 3.4.3.

The reasons why this method is so useful is that the reflection coefficient can be properly represented by a ratio and also it experimentally exhibits this bilinear transformation property. We want to use the bilinear transformation property which is expressed in reflection matrix as well as the scattering matrix properties. Therefore, it is important that the relationship between the scattering coefficient and reflection coefficient be shown.

Reflection Matrices

$$\begin{bmatrix} a \\ b \end{bmatrix} = \begin{bmatrix} t_{11} & t_{12} \\ t_{21} & t_{22} \end{bmatrix} \begin{bmatrix} a' \\ b' \end{bmatrix}$$

where



$$\frac{b}{a} = \Gamma \quad \frac{b'}{a'} = \Gamma'$$

Bilinear Transformation

$$\Gamma = \frac{t_{22} \Gamma' + t_{21}}{t_{12} \Gamma' + t_{11}} = \frac{A\Gamma' + B}{C\Gamma' + D}$$

Scattering Matrices

$$\begin{bmatrix} a \\ a' \end{bmatrix} = \begin{bmatrix} S_{11} & S_{12} \\ S_{21} & S_{22} \end{bmatrix} \begin{bmatrix} b \\ b' \end{bmatrix}$$



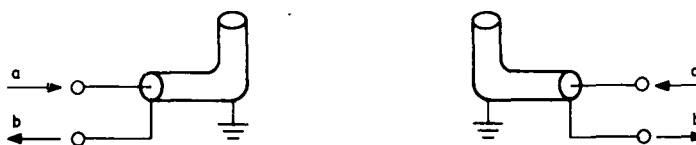
Bilinear transform expressed in terms of scattering parameters as shown by P. A. Deschamp (5) is

$$\Gamma = \frac{S_{11} + S_{12}^2 \Gamma'}{1 - S_{22} \Gamma'}$$

It seems reasonable that is lossy bilinear relationship can be applied to mutual coupling problems. Two adjacent antennas would appear as shown below when using reflection conventions,



and in terms of scattering convention as shown below.



Expressing the transformation from terminal 2 to terminal 1 is

$$\Gamma_1 = \frac{A \Gamma_2 + B}{C \Gamma_2 + D}$$

Application of the sliding short method to the two antennas permits measurement of the scattering coefficient.

Scattering Matrices

$$\begin{bmatrix} b \\ b' \end{bmatrix} = \begin{bmatrix} S_{11} & S_{12} \\ S_{21} & S_{22} \end{bmatrix} \begin{bmatrix} a \\ a' \end{bmatrix}$$

S_{11} is the reflection coefficient at terminal 1 when terminal 2 is matched.

S_{22} is the reflection coefficient at terminal 2 when 1 is matched.

S_{12} is the transmission coefficient from 1 to 2 and because of reciprocity $S_{12} = S_{21}$.

These parameters as measured for quarter wave dipoles above ground are shown in Figures 38, 39, and 40.

Transmission Efficiency

The ratio of power out terminal 1 to power in terminal 2

$$\eta = \frac{|S_{12}|^2}{1 - |S_{11}|^2}$$

The ratio of power out terminal 2 to power in terminal 1

$$R = \frac{|S_{12}|}{1 - |S_{22}|^2}$$

Insertion Loss

$$L = 10 \log \frac{P_1}{P_2}$$

where

P_1 = Maximum available power

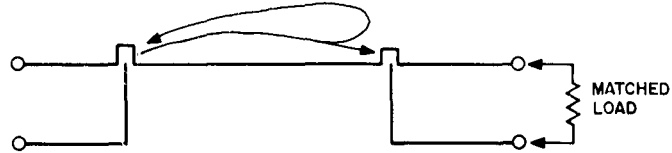
P_2 = Power delivered to matched load

$$L = 10 \log \frac{1}{(S_{12})^2}$$

$$L = L_R + L_D$$

where

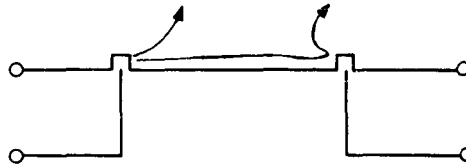
$L_R = -10 \log (1 - |S_{11}|^2)$ equals the reflection losses caused by the mismatch seen at terminal 1 when terminal 2 is matched. Thus this gives the effect the adjacent antenna has on the radiating antenna, as shown below.



$$L_D = -10 \log \frac{|S_{12}|^2}{1 - |S_{11}|^2}$$

equals insertion loss in antenna 1 and 2 plus radiation loss.

Since antennas themselves are nearly lossless, L_D can be considered losses due to radiation:



Results from the sliding short method for the coupling between adjacent dipoles antennas are given in Figures 38, 39, and 40. The mismatch at the input of the dipole feed was not tuned out when a change of separation distance was made. This is one of the reasons for the large discontinuity which is seen in Figures 38 and 39. Figure 41 shows coupling measurements made by a power meter resulting from returning both dipoles for each distance of separation.

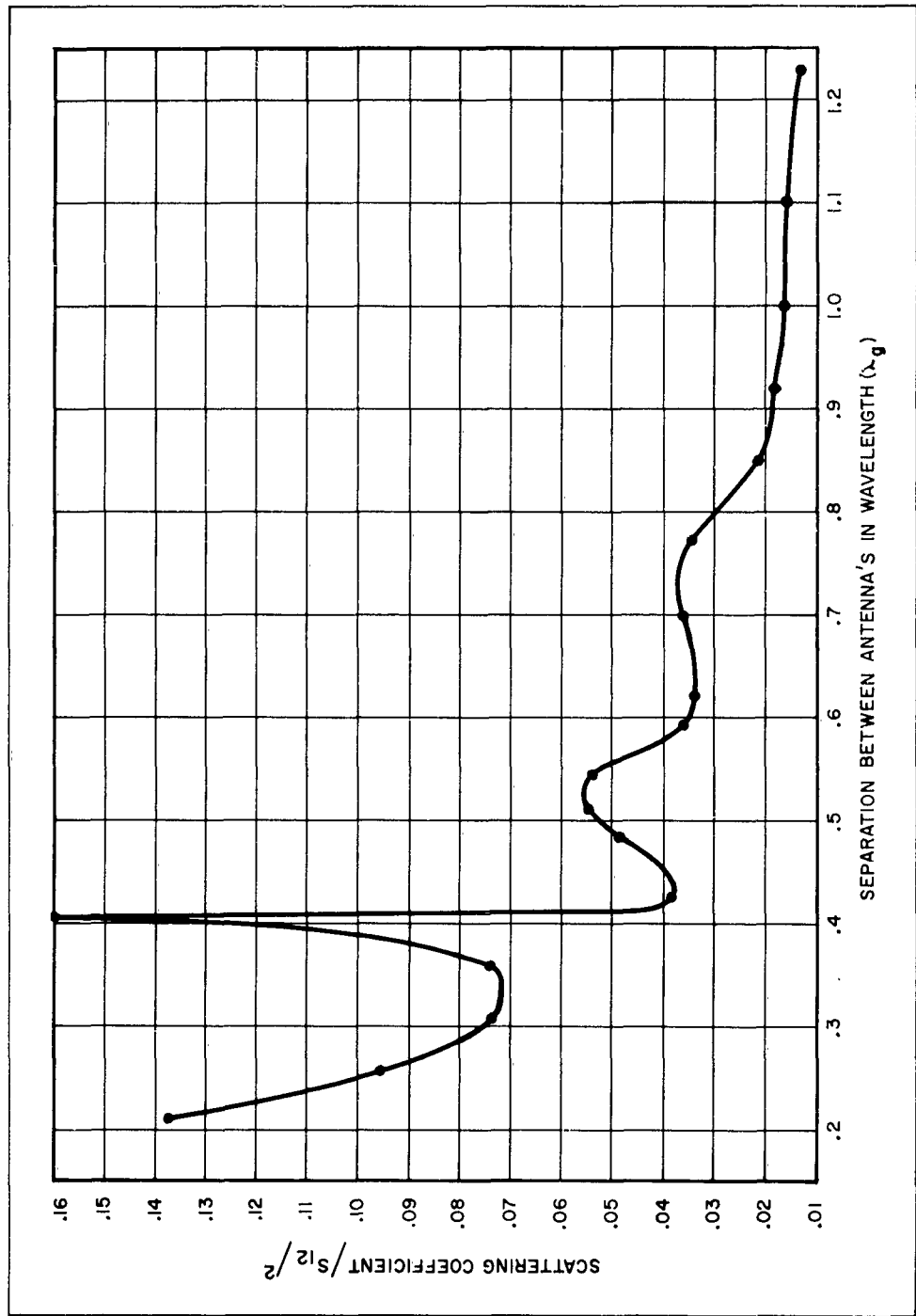


Figure 38. $|S_{12}|^2$ vs. Distance of Separation Between Dipoles

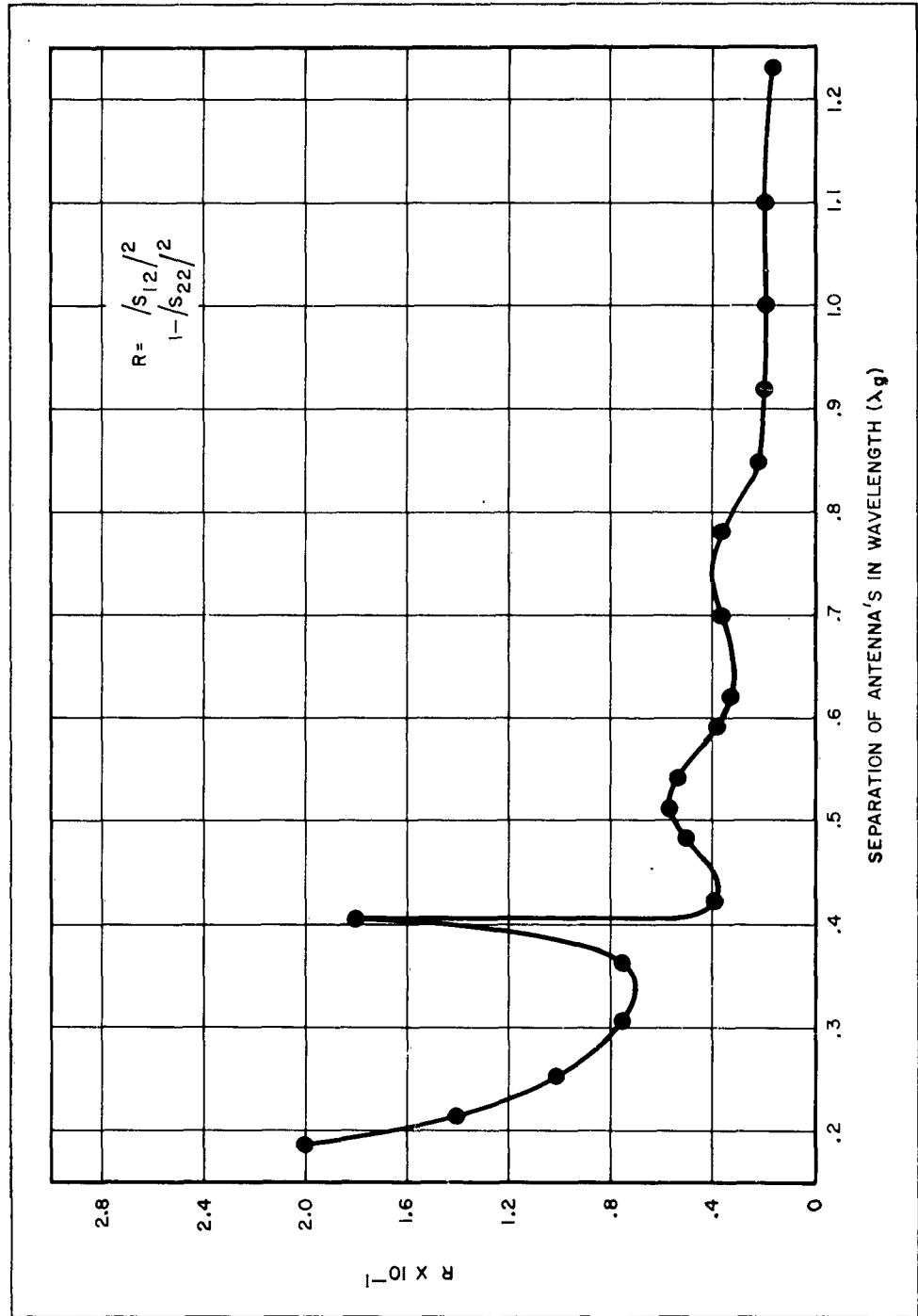


Figure 39. Transmission Efficiency

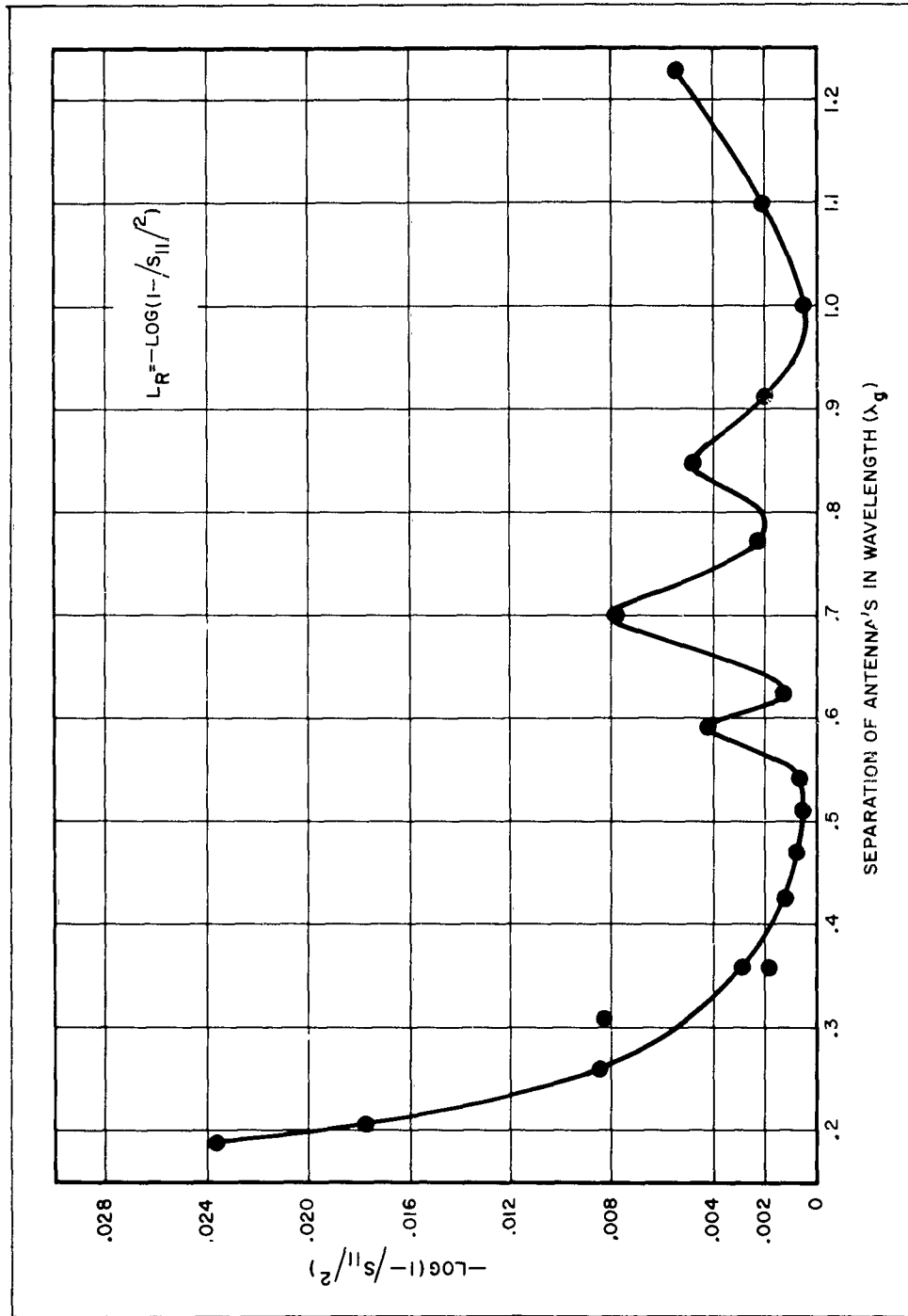


Figure 40. Reflection Losses in Antenna 1

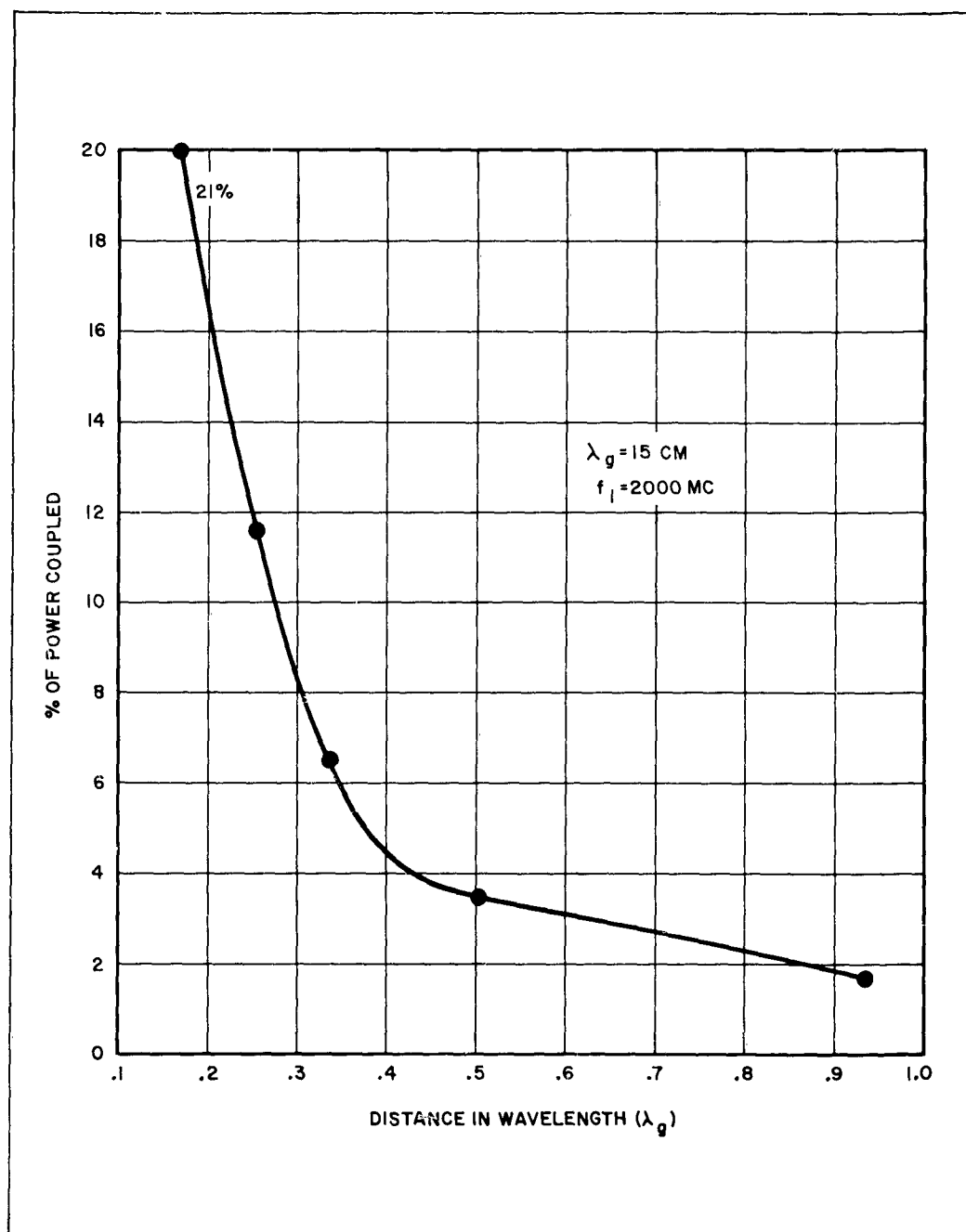


Figure 41. Power Measured By Bolometer Between Adjacent Dipoles

References

1. W. Altar, "Q Circles: A Means of Analysis Resonant Microwave System" Proceedings of IRE, Part I, May 1947, Part II, April 1947.
2. G. Deschamp, "Determination of Reflection Coefficient and Insertion Loss of a Waveguide Junction," Federal Telecommunications Laboratory, April 2, 1953.
3. E. F. Bolinder, Technical Report 312 and 344, Massachusetts Institute of Technology, R. S. of E.
4. J. E. Storer and L. S. Sheingold Stein, "A Simple Graphical Analysis of Two-port Waveguide".
5. G. A. Deschamp, "Near Zone Electromagnetic Waves," Report 8, Federal Communication Laboratory.